SELF ORGANIZED NANO SCALE ARRAYS FOR ULTRAHIGH DENSITY MAGNETIC RECORDING

By

Vinay Shankar Vidyarthi

DEPARTMENT OF MATERIALS AND METALLURGICAL ENGINEERING

Indian Institute of Technology, Kanpur

APRIL, 2004

SELF ORGANIZED NANO SCALE ARRAYS FOR ULTRAHIGH DENSITY MAGNETIC RECORDING

By

Vinay Shankar Vidyarthi

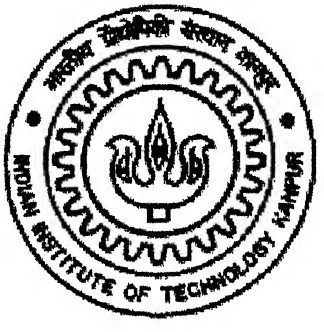

DEPARTMENT OF MATERIALS AND METALLURGICAL ENGINEERING

INDIAN INSTITUTE OF TECHNOLOGY KANPUR

APRIL 2004

CERTIFICATE

This is to certify that the work entitled **"SELF ORGANIZED NANO SCALE ARRAYS FOR ULTRAHIGH DENSITY MAGNETIC RECORDING"** by **Vinay Shankar Vidyarthi**, Roll Number: Y210633 has been carried out under my supervision and that this work has not been submitted elsewhere for a degree.

Dr. K. N. Rai
Professor
Department of Materials and Metallurgical Engineering
and Materials Science Programme,
Indian Institute of Technology
Kanpur-208016, India

DEDICATED

to

MY PARENTS

SISTER & BROTHERS

ACKNOWLEDGEMENTS

I express my deep sense of indebtedness and heartfelt reverence to **Professor K. N. Rai,** for his mentorship, and coaxing. I would never have been able to present this thesis in its present form without his inspiring guidance, unending encouragement and granting me personal freedom throughout my M. Tech programme.

Apart from the Academic knowledge, I have imbibed several day-to-day experiences from Prof. Rai. I take this opportunity to acknowledge that Prof. K. N. Rai has honored me by sharing several of his experiences by elucidating upon the various facets of life, which have indelibly stamped an ideology, which, I would treasure throughout my life.

I wish to express my earnest gratefulness to **Professor Jitendra Kumar** for his continuous guidance in experimental work as well as for my personal carrier related issues.

I would like to express my sincere gratitude to Prof. Jitendra Kumar, Prof. D. C. Agrawal, Prof S. Sangal, Dr. Asim Tewari, Prof. Y. N. Mohapatra, for transmitting valuable knowledge to me via courses, I have taken during my M.Tech programme.

I wish to extend my sincere thank to all the staff members of ACMS (Mr. A. Agnihotri, Mr. S. C. Barthwal, Mr. Sharma, Mr. Shiv Kumar, Mr. D. D. Paul, Mr. Jai Kishan, Mr. Umashankar, Mr. Kartikein and others) Mr. Somnath , Mr. V. P. Sharma and Mr. G. S. Thapa for their technical help during my experimental work.

Special thanks are due to Mamta for her at the spot help during my thesis preparation, and for making my stay a memorable one. Earnest thanks go to Murali and Rajeev for their technical help during experimental work.

I am grateful to Professor K. N Rai's family members who with their affection and love made me feel at my own home. I wish to take this opportunity to thank my all friends at IITK for their cooperation and making my stay enjoyable.

Finally, I am greatly indebted to my beloved family members, whose, continued encouragement, support and the patience they have shown during the programme enabled me to complete the study at ease.

I.I.T KANPUR

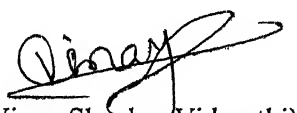

March, 2004 (Vinay Shankar Vidyarthi)

ABSTRACT

Anodic porous alumina template with regular pores of 45nm diameter has been developed by anodizing indigenous Aluminum in acidic medium. The pores of alumina template have been filled up with Nickel by electrochemical method. Characterization with regard to microstructure and magnetic properties has been carried out by techniques of Transmission Electron Microscopes and Scanning Electron Microscope, BET and Vibrating Sample Magnetometry. It has been observed that the anodization of aluminum foil in 0.3M oxalic acid solution at 40V DC produces pores of (I)circular (of 45±10 nm diameter)shape and size(II)with interpore spacing of 75±10nm having uniform (III) Self-ordered cylindrical shapes. BET-surface area measurement also confirms the pore sizes (44nm) measurement within close variation.

Further, a typical pulse electrodeposition process in an electrolyte (containing 300g/l $NiSO_4.6H_2O$, 45 g/l $NiCl_2.6H_2O$, 45 g/l H_3BO_3, pH 4.5) with a nickel coated Copper as counter electrode was employed to deposit Nickel in the pores of as made anodic porous alumina as well as commercial anodic alumina filter. The bulk magnetization hysteresis loop of arrays of Nickel nanomagnets at room temperature shows a coercive field, $H_C^{\parallel}$ =150 Oe, in a direction perpendicular to porous alumina sheet. The measurement in plane of the sheets produced a coercive field ($H_C^{\perp}$) of 25 Oe. This hysteresis loop indicates preferential magnetic orientation parallel to nano wire axis. The value of $H_c^{\parallel}$ measured for Nickel wire is at least a factor of 5-10 smaller than the values expected for a single domain wire magnetized parallel to the pore axis. This indicates that the resulting individual metal nanowire has multidomain characteristic. The feasibility of producing pores from thin film aluminum supported on copper thin film has also been examined

The pore density in the anodic porous alumina is of the order of 10^{11}-10^{12} pores/in^2. Assuming each pore filled with ferromagnetic material as one bit of information, the recording density of the present substrate is about 600 Gbit/in^2 .The current claimed capacity for advanced by manufacturers is around 100Gbit/in^2.

CONTENTS

List of Figures

List of Tables

CHAPTER 1

INTRODUCTION

Magnetic Data Storage has seen tremendous technological changes during the last 40 years and is expected to remain as the mainstream mass storage technology for many years to come. Magnetic storage plays a key role in the development of the modern era of information technology. Magnetic recording is principally responsible for the widespread, relatively inexpensive use of recorded sound and video images. Also, in conjunction with semiconductor technology magnetic recording has contributed significantly to the growth of computer development.

Magnetic recording requires suitable recording media (disks/floppy/tape) and sensitive signal detection heads. The recording systems have undergone development along two different lines [1]; fixed heads involving linear recording so called longitudinal recording and rotating head involving helical recording also known as perpendicular recording. While the first is useful for digital data and analog audio applications, the second is meant for video and digital audio applications. Linear recording has fast access and high throughput of data capability but the associated areal densities are rather low because of wide track widths. On the other hand, helical recording achieves very high areal densities but has slower access and poor transfer capacity.

Since 1991, the annual growth rate of the storage density for commercially available hard disks has been 60 %(shown in Figure 2.3). Nowadays, hard disks with an areal density of 35.5 Gbit/in^2 are commercially available, and a number of companies have demonstrated densities ranging up to 100 Gbit/in^2 in their laboratories. Currently, it

takes approximately two years from a laboratory demonstration to the market introduction. The increase in areal density in magnetic recording has mainly been achieved by scaling head and media parameters to smaller dimensions. Common approach is to reduce grain volume (V) to a limit where each grain represents a bit, keeping the transition noise within the tolerable limits. As a result, the thermal energy may start competing with the grain anisotropy energy (K_u V), due to superparamagnetic effects. This will limit the predicted storage capacity to about 70 Gbit/in^2 for longitudinal recording utilizing planer continuous films [2,3].

One approach to overcome this limit is via patterned perpendicular media [2–6], where one bit of information corresponds to one single-domain nanosized particle, a so-called nanomagnet. Since each bit would be composed of a single high-aspect particle, the areal density of this patterned media can, in principle, be more than one order of magnitude higher than in conventional longitudinal media. For example, an areal density of about 300 Gbit/in^2 can be achieved by a hexagonally arranged array of nanomagnets with a lattice constant of about 50 nm. Moreover, the nano-wire arrays offer the advantages of perpendicular magnetic anisotropy useful in perpendicular recording, square hysteresis loops, high coercivity and almost quantum read-write characteristics due to nearly single-domain nature of the wires.

Conventional method to obtain arrays of nanomagnet is based on expensive lithography techniques such as electron beam lithography and ion beam lithography. The cost of lithography increases as the size of the particle goes down to nanometer scale and especially when high density nano-arrays are needed. Moreover, the restricted growth of

the particle in the third direction limits the flexibility of obtaining high aspect ratio particles.

One promising technique to obtain nanomagnet arrays is based on self-organized hexagonally-arranged porous alumina templates [7]. This method is very cheap as compared to lithography technique. In this one can have tailor-made magnetic particles arrays with large aspect ratio on a large area by electrochemical methods. Porous alumina template has already been subject of scientific and commercial interests for last 30years [8-15]. It has created commercial interest because of its applications for the fabrication of plethora of nanoscale devices [16]. It has been subject of interest in the scientific community because it can be used to study the properties of materials at low dimensions. In the present study, interest in this has been stimulated mainly because of its possible application for ultrahigh density magnetic recording media.

In the past, researchers have focused their attention to develop hexagonally ordered arrays of pores in alumina from highly pure (99.999 %) Al. Highly pure Al is very expensive as compared to indigenous Aluminum (maximum purity ≈ 99.7%). For example, 10μm thick (100mm X 100mm) Al foil with purity 99.999% from Goodfellow costs US $ 441,whereas 10μm thick (9m X 300mm) Al foil with purity 99.5% from Hindalco or other Aluminum manufacturing Industries of India costs only US $ 1. In the present investigation, efforts therefore have been directed to study the anodization behavior of less pure Aluminum foil.

In the present study, focus has been directed to the followings:

- Introduction to the theory of Magnetic recording
- Suitable media for perpendicular recording
- Thermodynamic stability of nanomagnets
- Mechanism of pore formation during potentiostatic anodization of Aluminum.
- Development of ordered porous alumina template from commercial Aluminum
- Filling of pores of Alumina template with ferromagnetic magnetic materials by the method of electrodeposition
- Feasibility of the process to the industry

CHAPTER 2

MAGNETIC RECORDING AND MATERIALS CHARACTERISTICS

2.1 BASIC PRINCIPLE

In order to deal with the requirements imposed on materials for recording media, it is imperative to describe the basic principle of magnetic recording itself. Any information, be it sound, images, or numerical data is expressed as a time varying electrical current and magnetic flux. The recording head consists of

(I) a small coil, through which the signal as current passes, and

(II) a grapped soft magnetic structure that intensifies and localizes the resulting magnetic flux.

The conventional recording medium consists of a substrate (tape or disc) coated with magnetic film/particle that moves relative to the head in close proximity below the the gap. The head field magnetizes the magnetic coating species according to the signal current in the coil such that the time varying electrical signal gets converted into a spatially varying magnetic pattern along a track on the medium surface. A reversal of the current causes flip over and produces transitions between regions of opposite magnetization. The read back process involves movement of the tape surface once again over the head. Now, the field of the magnetized region gives rise to a magnetic flux in the coil. Thus, on relative motion between the head and the medium, voltage gets induced in the coil in accordance with the changes in magnetization of the medium. This spatially varying pattern is converted back into a time varying electrical signal giving rise to

processed information. In magnetic recording, the encoding of information can be analog or digital type. This process of magnetic recording should be a precise representation of the incoming stream of information so that the signal obtained on reading back gives an exact reproduction of the original. Digital recording involves the breaking of each flux reversal into discrete number of electrical pulses assigning value of one or zero at each neighborhood of flux reversal, which are then recorded. But in the event of analog recording, flux variations are simply converted into time varying electrical output. While, the analog recording has been widely used to store audio and video information, the digital recording is confined to data storage. This picture is, however changing fast and digital recording is now being used increasingly in audio and video recording as well. Digitalization offer immense possibility of making dynamic corrections in reconstructing the copies of repeated original informations. Whether the recording method is analog or digital, quite similar (though not identical) requirements have to be met of the recording materials.

The improvement in storage density is not only due to the development of magnetic media. The role of development in recording/reading heads is in no way insignificant when we talk of high density storage media. Apart from the media capacity to store at high areal density, there are several requirements that have to be met for optimum performance. All reading/recording and electronics should be compatible with the media so as to obtain optimum signal to noise ratio. In this way, development in recording media is co-ordinated with the development in recording/ reading heads.

Both the longitudinal and perpendicular writing heads (integrated with GMR/spin valve Reading Heads) are shown in figure 2.1 and figure 2.2 respectively.

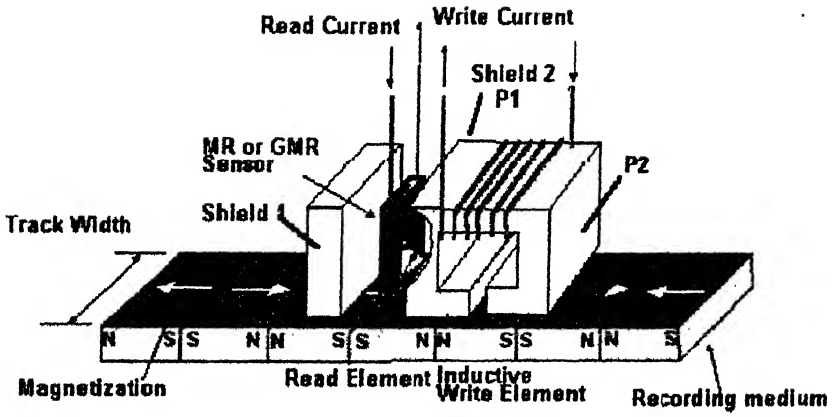

FIGURE.2.1: LONGITUDINAL RECORDING PROCESS

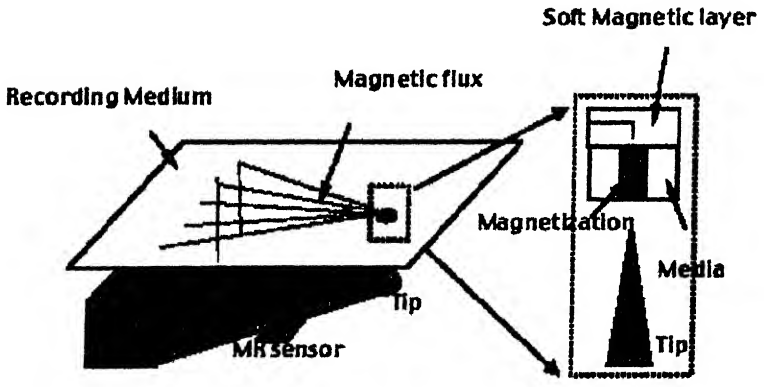

FIGURE 2.2: PERPENDICULAR RECORDING PROCESS

Each head is a device which converts, through inductive mechanism, time varying electrical signal (of audio/video data file) into a set of time varying magnetic flux ripples (transitions). The aforementioned principles, in general, are applicable to both types of magnetic recordings. However, there are some requirements which are specific to a particular type of recording (longitudinal and perpendicular). Because of fundamental importance of these two processes of recording to improve the areal density of media, these are being discussed in more detail in the following sections.

2.1 LONGITUDINAL RECORDING

In case of longitudinal head, flux transitions pass parallel to magnetic media surface (supported on polymeric tape or disc), which moves at a desired speed. The magnetic media surface is generally thin layer of hard magnetic material coated on a suitable substrate. This coating consists of fine magnetic grains or domains, which serve as memory storage cells. These become longitudinally magnetized when a strong magnetic field is applied along the layer plane. The magnetic field is created by the signal fed to the recording head. As a consequence, the magnetic domain just below the head gets magnetized in the direction of the field. When a reading head passes through this magnetized surface, a change in flux is observed. According to Faraday's second law of magnetism, an induced emf is produced in the head coil when the head passes through the magnetic layer. In this way, the reading head senses the direction and magnitude of the magnetization and reproduces the recorded signal. A single head can perform both read and write functions.

2.2 PERPENDICULAR RECORDING

Perpendicular magnetic recording is fundamentally characterized by demagnetizing field free transitions. This requires neither both too small thickness and saturation magnetization nor extremely high coercive force for the media to obtain a small transition width. Although, these were pointed out from the complementary relationship with longitudinal recording from the beginning of perpendicular recording study [17], the demagnetizing field free characters of the transitions become to have significant meaning for high density recording. High saturation moment and a certain thickness of the media is still required in forthcoming ultra-high density recording for obtaining enough output from tens nano meters order small bit cells. These are also essential to maintain thermal stability of the recorded magnetization. For reasons, researches on perpendicular recording media have been performed for a long time.

In case of perpendicular recording head, signal flux passes perpendicular to the surface as stored data. The magnetic material is magnetized normally to the substrate surface. In this way, a single magnetic grain covers a very small surface in comparison to longitudinal recording media. The volume of the grain is along the direction, perpendicular to the surface in cylindrical shape.

A comparative list of conditions for longitudinal and perpendicular recording generally employed or achieved [18] is produced in Table-2.1.

Table-2.1: COMPARISON OF LONGITUDINAL AND PERPENDICULAR RECORDING PROCESSES

Recording Type	Longitudinal	Perpendicular
Magnetic Noise	1)Demagnetization field 2)Transition	Free from Demagnetization Transition noise
Hysteresis Squareness	$M_r/M_s \approx 0.8$	$M_r/M_s \sim 1$
Pole Tip B_s	20KOe	20KOe
Maximum Anisotropy Field	$H_k \approx 10.6$KOe	$H_k \approx 16$KOe$-4\pi M_s$
Minimum in Plane Parameter	$D = \sqrt{\frac{2SkT\ell n(tfo/\ell n2)}{HkMrt(1-2Hd/Hk)^{\frac{3}{2}}}}$	$D = \sqrt{\frac{2SkT\ell n(tfo/\ell n2)}{HkMrt(1-2Hd/Hk)^{\frac{3}{2}}}}$
Transition Parameter	$\frac{a}{D} \approx 0.5$	$\frac{a}{D} \approx 0.5$
Memory density	Moderate	Higher

In both types of recording systems, storage limits are mainly determined by the decay of signal to noise ratio (SNR) due to thermally induced magnetization fluctuations. The essential argument which holds true for both type of recording is that the SNR varies inversely both as (powers of) the grain diameter and the recording density. Thermally induced signal decay increases with decreasing grain volume. Therefore, perpendicular media have larger limiting density at a given SNR, because, it is optimized by tall grain (high aspect ratio) with small in-plane diameters (about 5:1). The longitudinal recording has a smaller limiting density because optimal thickness equals the in-plane grain diameter.

2.2 MAGNETIC MEDIA REQUIREMENTS

The primary characteristics required of the magnetic materials for use in recording media can be summarized as follows: The retained magnetization intensity (or retentivity) should be sufficiently high as it determines the strength of the field sensed by the read back head. The retentivity depends on the intrinsic magnetization of the media material and the preferred directions therof. The another property relates to the field strength needed to cause magnetic reversal of the material and is generally characterized by the coercivity (H_c) , i. e., the field where slope is maximum in the magnetization curve. The coercivity (H_c) value must not be so large as to prevent successful writing and possibly overwriting or erasure by available heads. It must, however, be large enough to resist unwanted changes or degradation of the signal caused by the internal or self-demagnetizing field during storage. This field is proportional to the magnetization intensity of the media itself, the coercivity needs to be high in strongly magnetizable coatings. The internal demagnetization field is important principally at high densities of magnetic transitions, where, opposite magnetic poles in the recorded patterns are in close proximity to each other. Higher coercivity, the breadth of the dM/dH versus H curve (Figure 2.4) is also crucial. This is commonly expressed by the switching field distribution (SFD). A narrow SFD clearly facilitates the writing of sharp and well-defined magnetic transitions and hence contributes to the ability to record information at high densities. A broad SFD not only corresponds to diffuse transitions but also indicates a variety of adverse effects, e.g., problems in erasure, overwriting, etc. The appropriate SFD is important in systems requiring thorough erasure using special heads (e. g. analog) and in others where some residual overwritten signal can be tolerated but no erase head is used (e.g., digital).

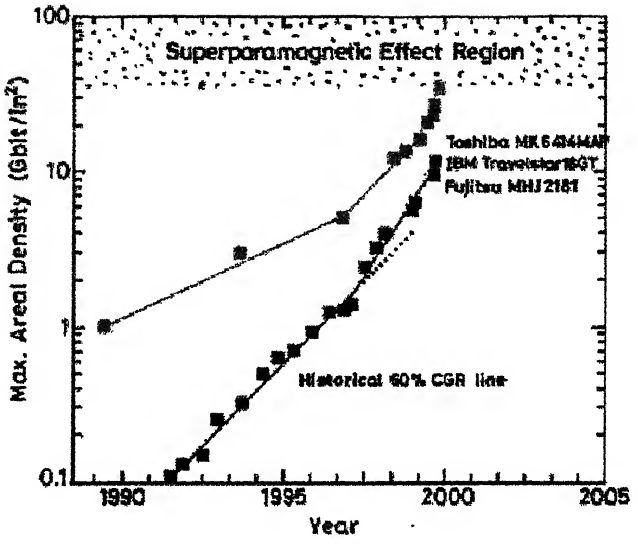

Figure 2.3 Super paramagnetic limit (red color) threatening 60% compounded growth rate line (green color) of recording density.
[Diete Weller & Andreas Moser IEEE Trans. Magn. 35(1999)4423]

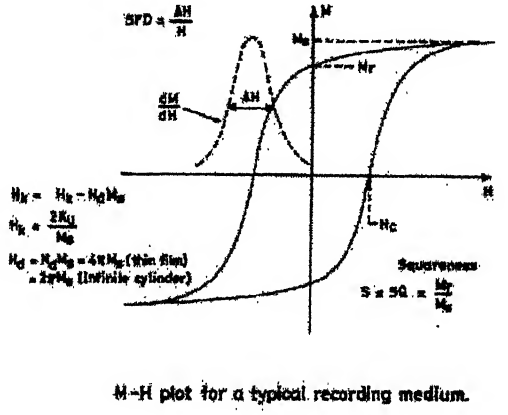

Figure 2.4 Hysteresis loop (plot of magnetization M versus applied field H) for a typical recording medium

2.3.1 Memory Density and Supported Materials

Improvement in magnetic memory density has followed parallel developments in electronic technologies and processing. These mainly include (a) development in electronic circuitry and signal processing (b) developments in miniaturization of writing/recording heads for longitudinal and perpendicular recording composite heads (c) development in newer magnetic materials and (d) development in substrates for supporting magnetic particulate/thin film along with associated (e) development in materials processing technologies. As a result memory density has improved continuously with 60% compounded rate [19] as shown in Fig1.These developments have been based on realistic vision [20-2].The one important aspect of the present work is concerned with magnetic media behavior and support material processing. The support /substrate, the magnetic media particulate /thin film and the writing-reading heads are all coupled through magnetic flux and mechanical constraints. It is thus important to realize that the optimum performance is not independently connected to anyone of these separately. A coordinated operation of these will yield desired result. Thus, each of these is discussed in foregoing sections here.

2.3.2 Magnetic Media

Here magnetic media means magnetic particulate or thin film only. These have to satisfy many requirements of recording and storage life. While, some of the required features depends upon materials chemistry, the others depend upon shape and size of magnetic material. Some of these, important to ultrahigh density requirements are listed below one by one

2.3.1 Memory Density and Supported Materials

Improvement in magnetic memory density has followed parallel developments in electronic technologies and processing. These mainly include (a) development in electronic circuitry and signal processing (b) developments in miniaturization of writing/recording heads for longitudinal and perpendicular recording composite heads (c) development in newer magnetic materials and (d) development in substrates for supporting magnetic particulate/thin film along with associated (e) development in materials processing technologies. As a result memory density has improved continuously with 60% compounded rate [19] as shown in Fig1.These developments have been based on realistic vision [20-2].The one important aspect of the present work is concerned with magnetic media behavior and support material processing. The support /substrate, the magnetic media particulate /thin film and the writing-reading heads are all coupled through magnetic flux and mechanical constraints. It is thus important to realize that the optimum performance is not independently connected to anyone of these separately. A coordinated operation of these will yield desired result. Thus, each of these is discussed in foregoing sections here.

2.3.2 Magnetic Media

Here magnetic media means magnetic particulate or thin film only. These have to satisfy many requirements of recording and storage life. While, some of the required features depends upon materials chemistry, the others depend upon shape and size of magnetic material. Some of these, important to ultrahigh density requirements are listed below one by one

2.3.3 Magnetic Anisotropy

The nature of magnetization strongly depends on magnetic anisotropy. It is defined as the energy per unit volume required for turning the magnetized state by 90° from its easy direction. It is also called crystal magnetic anisotropy or magnetocrystalline anisotropy. The direction of stable internal magnetization (or easy direction) in hexagonal cobalt is along its c-axis, the anisotropy increases with an increase in rotation angle Φ (the angle between the c-axis and the final internal magnetization). It takes its maximum value at Φ =90° and then decreases to its original value at 180°. This energy can be expressed as

$E_a = K_{u1} \sin^2 \Phi + K_{u2} \sin^4 \Phi + \ldots\ldots\ldots$

Where K_{u1}, K_{u2}, ...are constants. Usually the first term is sufficient to express the actual anisotropy energy. Thus the maximum value E_a becomes just K_{u1} itself for $\Phi = 90°$. The stored magnetic energy is just K_uV, if V is the volume and K_u is taken as anisotropy energy density.

2.3.3.1 Maximum Longitudinal Anisotropy

For longitudinal recording optimal, recording occurs when the deep gap field is approximately three times the coercivity:

$H_{dg} = 3H_c$

Since, $Hc \approx 0.5H_k$ $S = M_r/M_s \approx 0.8$

Using the above equation, we get

$H_k = 10.6KOe$

2.3.3.2 Maximum Perpendicular Anisotropy

Perpendicular media exhibit sheared loops. For a virtually square intrinsic loop, the sheared loop squareness S^* is given by:

$S^* = 1 - 4\pi M_s/H_k$

For an efficient pole structure, the maximum deep gap field should be sufficient to saturate the medium or "close to loop." When the film were away from the write pole, this field is $H_k = 16kOe - 4\pi M_s$

2.3.4 Magnetic Media Life

There are two aspects. Threat to storage life due to environmental or mechanical causes by attacking chemical and structural integrity .This can be avoided by suitably modifying the manufacturing process. This does not have much effect on storage density of media. The other important cause is the thermodynamic constraints on existence of ferromagnetic coupling. If the grains/particulate size is too small, the signal stored in form of magnetized domain decays with time and is lost after a definite lapse of time due to thermal randomization effect and material becomes super paramagnetic. There is a definite relation [23] between decay of magnetization M_r, the time lapsed 't ', relaxation time ' r ', the jump frequency for decay f_o, the temperature T (K) and associated energy barrier $E_{Bo} = (V^*K)$ as given below

$$t = f_O Exp\left(-\frac{E_B}{kT}\right) \quad \text{---------- (1)}$$

Assuming a life (t) of 10years at T=350K

$$\frac{E_B}{kT} = \frac{V^* K}{kT} \approx 40 \qquad \text{---------- (2)}$$

Here K is anisotropy constant and V^* is activation volume or critical volume. Thus ferromagnetic particles smaller than V^* will loose their magnetization and become superparamagnetic. Thus the diameter of a stable particle of Co with $K = 4.5 \times 10^6$ erg/cm^3 and M_s=1400 emu/cm^3 should not be smaller than 7.7nm. Table 2.3 shows the critical activation volume and size for common magnetic media. The above equation does not account for magnetic field (i.e. H =0). However, recorded media contain magnetized domains which are associated with their self demagnetizing field H_d (Fig. 2.5). This field aids the thermal decay process. As a result, particle size of recording media will still be larger than one predicted by equation (2). The field dependent barrier height E_B is given by expression

$$E_B(H) = E_{Bo}(1 - H/H_O)^m \qquad \text{========== (3)}$$

Where, H_o is switching field without thermal fluctuation.

Table 2.2 is the list of intrinsic properties of common magnetic media.

2.3.5 Switching Fields

This relates to head field, H_{dg} of the writing pole gap. This must surpass the coercive field H_c of the magnetic media. While, materials with very high H_c are needed to enhance storage life and demagnetizing effects from stray field, a too high value is also unwelcome, because head field larger than 2T ≈ 5000Oe is difficult to achieve. Apart from these contradictory requirements, H_c value heavily depends upon shape and size of magnetic media particulates, which, in turn also decide functioning parameter and

approachable memory density. A reasonable relation between H_c, H_k (anisotropy field), saturation magnetization M_s and demagnetizing field coefficient N_{eff} can be expressed as

$H_c = \alpha H_k - N_{eff} M_s$

Where, $H_k = 2K_u/M_s$ and $\alpha = 1$

The dependence of H_c on shape and size is due to the dependence of demagnetizing field and of magnetization reversal on size. For small diameter(single domain) cylindrical particulate, the reversal is due to coherent Domain Rotation(i.e. independent of diameter size) and for large diameter, the reversal is by curling .Assuming curling mechanism of reversal [24] H_c has the dependence on wire diameter d_w as

$$H_C = \frac{2\pi (2.08)^2 A}{M_S d_w^2}$$

Here, $(2.08)\ A^{1/2}/M_s$ is critical diameter beyond which curling mechanism becomes operative.

2.3.6 Switching Field Distribution

The switching medium field, H_c (coercive field) is not the only sole material characteristic which controls the recording process. A large distribution in switching field means difficult erasure or re-writing on one end and print through effect [25] on the other end. In contrast to this a sharp distribution means well defined sharp recording of signals (transitions) enabling high density information storage. Figure 2.4 explains the relation between H_c squareness 'S' and switching field distribution 'SFD' [25]associated with a hysteresis loop.

Table-2.2: INTRINSIC PROPERTIES OF COMMON MAGNETIC MEDIA

Materials	T_c (k)	M_s(emu/cm^3)	K_u(10^7erg/cm^3)	H_k (KOe)	γ(erg/cm^2)
Fe	1043	1714	0.048	0.56	2.9
Co	1404	1400	0.45	6.4	8.5
Ni	631	484	0.005	0.207	0.7
FePd	760	1100	1.8	33	17
CoPt	840	800	4.9	123	28
FePt	750	1140	6.6 -10.0	116	32
MnAl	650	560	1.7	69	16
CoPtCr		298	0.2	13.7	5.7
Co_3Pt		1100	2.0	36	18
$Fe_{14}Nd_2B$	585	1270	4.6	73	27
$SmCo_5$	1000	910	11.0 - 20.0	240-400	42-57

Table-2.3: CRITICAL DIMENTIONAL PARAMETERS

(ACTIVATION VOLUME, SIZE) OF COMMON MAGNETIC MEDIA

Materials	V_p (10^{-19} cm^3)	L_d (nm)	L_p(nm)	D (nm), r = 20	D (nm), r = 50
Fe	42.85	1.7	16.24	6.49	4.78
Co	4.572	7.47	7.7	3.08	2.27
Ni	411.4	5.14	34.52	13.78	10.15
FePd	1.14	24.2	4.85	1.94	1.43
CoPt	0.42	75.4	3.48	1.39	1.02
FePt	0.312-0.206	42.4	3.15-2.74	1.26-1.09	0.93-0.80
MnAl	1.21	87.9	4.95	1.97	1.45
CoPtCr	10.287	110.6	10.09	4.03	2.97
Co_3Pt	1.029	25.6	4.67	1.87	1.38
$Fe_{14}Nd_2B$	0.447	28.8	3.55	1.42	1.05
$SmCo_5$	0.187-0.103	93.6	2.65-2.18	1.06-0.87	0.78-0.64

$K V_p = 43kT$,

$L_p = (43kT/K)^{1/3}$ (CUBIC SHAPE)

$$D = \left[\frac{4V_p}{\Pi r}\right]^{\frac{1}{3}}$$

r =Aspect ratio (L/D)

(Cylindrical Particle)

$$L_d = \left[\frac{1.7\gamma}{\Pi^2 M_s^2}\right]$$

2.3.7 A Ultra High Reversal (Switching)

At present data processing rate of 300-400Mbit/s is not uncommon. Thus high speed magnetic recording [26] means domain reversal at nano second rate. Further improvement in data acquisition rate will demand response time better than subnano second. Magnetization reversal at such high rates indicates dominance of spin precession (gyromagnetic) effects. These indicate that studies employing nanosecond/picosecond pulse magnetization at high fields of the order of 20KOe is needed. Work in this direction has been done by Siegmann group[27-30] using picosecond pulses in perpendicular and longitudinal geometry, respectively indicating the need of higher switching fields (~20000Oe) for perpendicular reversal and lower field (~2000 Oe) for longitudinal reversal. Final stage of reversal, after terminating the pulse, was attributed to spin-Lattice damping. These workers have used internal field (demagnetization field) assisted magnetization reversal .Such concept will considerably affect the future head designing.

2.3.8 Media Noise

In general media noise has two contributions: the transition noise and the background or "DC" noise. For the high squareness media, the transition noise generally dominates. The transition noise is largely composed of an "effective" jitter term [31] that depends on the transition parameter, the cross track correlation width and the recording width. The cross track correlation width in fact depends strongly on the intergranular exchange interaction and the grain size distribution

2.4 Magnetic Media Substrate

Substrate carrying magnetic media has great influence on performance of media density. Smooth substrate allows even coating of magnetic layers with equiaxed grains enabling reproducible SNR with predictable results. Substrates are many polymeric tapes, metallic /glassy disks. Magnetic media is coated on these using electrolytic/sputtering techniques as intermediate layer protected by bottom coating for latter adhesion and top coating as antiabrasive lubricating layer. Vision from ultrahigh density recording and thermal stability requirement has lead to search substrate which allows circumventing the superparamagnetic limits. Self organized ordered porous alumina support is one of these [32-36]. The method of preparation of these is the part of present investigation.

CHAPTER3

LITERATURE REVIEW

3.1 ANODIC POROUS ALUMINA

Anodic porous alumina exhibits a homogeneous morphology of parallel pores which grow perpendicular to the surface with a narrow distribution of diameters and interpore spacing; the size of which can be easily controlled between 10 and 500nm [37]. Because of these properties, it has recently attracted increasing attention as a key material for the fabrication of devices on a nanometer scale, such as electronic and photo electronic devices, and for application in ultrahigh magnetic recording, micro filtration and ultra filtration[38-40] .

The geometry of anodic porous alumina may be schematically represented as a honeycomb structure which is characterized by a close-packed array of columnar hexagonal cells. Each hexagonal cell contains a central pore normal to the substrate, as shown in figure 3.1 [41,42]. However, the geometry of the anodic porous alumina usually obtained is far from the idealized model. This means the cells are irregular polygons, and the arrangement or the cells and pores is not ideal hexagonal.

Anodic porous alumina has been subject of wide research for more than 45years. Diggle, Downie and Goulding [43] have reviewed anodic oxidation of aluminum and described conditions required for the formation of pores in growing alumina film. Accordingly, the pore density (ρ_{pore})per $Å^2$ is given by

$$\rho_{pore} = \alpha(D_p + \beta V)^{-2}$$

In the above, α is the constant of proportionality equal to 1.15, D_p is the pore diameter varying with the acidic medium, temperature, pH and anodization voltage (though weakly), and β is another constant that depends on the acid medium and temperature. Thus, 15% sulfuric acid solution produces a pore density of $1.5x10^{11}/cm^2$ at the anodization voltage of 10V. The values of various parameters observed for porous alumina formed in different acidic medium are listed in Table 3.1

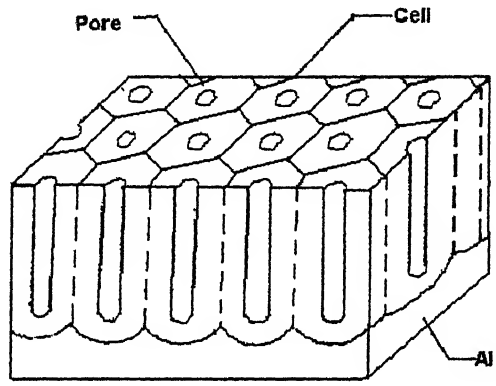

Figure 3.1: Schematic model of ideal porous structure of anodic alumina

Table 3.1 Values of various parameters for porous alumina formed in different acidic medium [43]

Acidic medium	T(°C)	D_p(nm)	β (nm/V)
15% Sulfuric Acid	10	12	1.6
2% Oxalic Acid	24	17	1.9
3% Chromic Acid	38	24	2.2
4% Phosphoric Acid	24	33	2.0

Sullivan and Wood [42] have produced alumina membrane containing self-organized nanostructure of pores (diameter 5-500nm) by anodic oxidation of aluminum in 1970. Now, this is used as a template to grow nanomaterials.

In 1975 Rai and Ruckenstein [44] had produced quite regular hexagonal cylindrical parallel pore arrays in anodic porous alumina by anodic oxidation of highly pure aluminum (purity 99.999%) in 0.6M oxalic acid solution. They have shown that cell size of hexagonal pore arrangement is directly proportional to the applied anodic voltage. They have also pointed out the dependence of pore density and anodization rate on the applied voltage.

Thomson and Wood [45] with the help of microanalysis of the regions comprising the cell material of the film formed in four different acidic electrolytes(sulfuric acid, oxalic acid, chromic acid and phosphoric acid) have investigated steady-state film growth rate for anodizing at constant voltage conditions in these acid electrolytes. Different growth rates were found in different electrolytes.

Till 1990s there have been very limited progresses in obtaining highly ordered pore structures, which would be useful in fabricating Nanoscale structures. After Masuda and Fukuda [46] in the year 1995 have reported that the pore regularity can be improved by a long anodization time under appropriate conditions, there has been a satisfactory progress in obtaining ordered pore structure. Long period anodization at 40 V in 0.3M oxalic acid electrolyte improved the regularity of the cell arrangement and produced an almost ideally arranged honeycomb structure. The defect free regions appear in large domains, whereas defects can be found on the boundaries of these domains. The size of the

domains is dependent on the anodization time. This means, size of the defect free regions increased with the anodization time. The long period anodization rearranged the cells and reduced the number of defect and dislocation. Masuda and Satoh [47] also showed that, after stripping away the thick oxides obtained from the first long anodization, a thin alumina film with highly ordered pore can be obtained by a subsequent re-anodization. The group of H. Masuda [48] has also studied the self-ordering of cell arrangement of Anodic Porous alumina formed in Sulfuric acid solution. The most appropriate potential for cell ordering was 25 to 27V in case of H_2SO_4 (0.3M) electrolyte. The concentration of electrolyte and temperature of the solution do not clearly affect the self-ordering of the cell arrangement. An ordered structure could be observed only at the bottom of the film. For the fabrication of the symmetrical films with straight holes throughout the entire film a two-step anodization process can be used. In this process, the concave texture of the Aluminum surface which is formed by selective removal of the film after the first anodizing step can induce ordered formation of pores even at the initial stage of anodization in the second anodizing step. Based on the idea of concave texture after the first step anodization, highly ordered monocrystalline nano channel-array architecture has been produced with the help of nanoindentation [49]. Idea was that if the development of the hole is guided by the appropriate texture of the surface at the initial state of anodization and an appropriate condition is maintained for the self-ordering the long range ordered array architecture can be expected to grow spontaneously. The anodization process is independent of the orientation of the Aluminum crystal, because the main driving force in the formation of channel in the anodic alumina is the electric field rather than crystal direction. Shallow predetermined concaves can initiate the pores and guide

the growth of the long channel. During anodization, pore interval (d) obeys the relation: d α 2.5nm/V. The naturally occurring ordering is presumably strongly dependent on the applied voltage compared to the growth using pre texturing, because the rearrangement of the cell configuration through growth must take place, in contrast to the ordering with texturing in which the pore can develop orderly in the initial stage of anodization.

Jessensky et al. [50] have extensively studied the morphology and formation conditions of ordered hexagonal pore arrays in anodic porous alumina. They have examined the influence of the pretreatment (annealing and electropolishing, surface roughness) of the aluminum substrate and the anodizing conditions on the growth kinetics. Homogeneous etching conditions are required in order to obtain regular pore arrays. Hexagonal pore arrays are related to a smooth etching front and a homogeneous depth of neighboring pores. One necessary condition for the formation of ordered pore arrays is the annealing of the aluminum foils before anodization in order to enhance the grain size in the metal substrate. The formation of ordered pore arrays shows that the process of self-organization is disturbed by a large number of grain boundaries in the nonannealed aluminum foils. Since the conditions for oxidation at the grain boundaries are different from those in perfectly crystalline areas, a different pore growth rate, leading to a rough etching front and a non ordered pore lattice is expected. Also the stirring of the electrolyte during anodization is a necessary condition for obtaining ordered hexagonal structures. They have shown that the pores start growing at the upper surface at almost random position. But, nearly perfectly ordered densely packed hexagonal structures can be observed at the bottom of the layer. Pore density in ordered pore arrays is typically about 20% lower than that at the upper surface of the alumina. This indicates that part of

the pores stops growing either shortly after their nucleation or during the self-organization.

Li et al. [51] has reported that the best ordering of pores in porous alumina is obtained when the expansion during anodic oxidation of aluminum is around 1.4. This expansion factor of 1.4 is independent of electrolyte used. They have produced ordered domain with rather large interpore distance (420nm) using higher voltage (160V) and 10wt % phosphoric acid solution as electrolyte. The values of expansion factor calculated from the experimental observation during the anodic oxidation of aluminum in different electrolyte is listed in the table 3.2

Table 3.2 Values of expansion factor under different anodization conditions which lead to the self-ordered hexagonal pore arrangements. [51]

Electrolyte (acid)	Concentration (Wt %)	Voltage (V)	Temperature (°C)	Expansion factor (%)
Oxalic	2.7	40	1	1.42
Sulfuric	20	19	1	1.41
	1.7	25	10	1.4
	1.7	25	1	1.36
Phosphoric	10	160	3	1.45

In contrast to Li et al. [51]'s reports, H. MASUDA et al. [52] has observed that the most appropriate condition is 195V at 0°C, in 0.3M H_3PO_4 solution. They (H. Masuda et al.) have claimed that at 150V, no self-ordering was observed and at 180v self-ordering was low. They have shown for the first time the conditions for promoting the self-ordering of anodic porous alumina with a large cell size of 500nm formed in phosphoric

acid solution, which is known to meet the conditions for anodization at high applied voltage. Temperature and concentration of the electrolyte used don't have much effect on the ordering of pores during anodization. All these investigations for producing ordered pores in anodic porous alumina have been done with high purity Aluminum (purity ≈ 99.999%). In the present investigation, indigenous Aluminum has been used as the starting material.

Recently, it's been reported that self –ordering requires a porosity of 10%, independent of the specific anodization conditions [53]. This corresponds to a volume expansion of aluminum to alumina of about 1.2.

The self-ordering of porous alumina with any interpore distance is possible if the applied potential and the pH value of the electrolyte match the 10% porosity rule [53]. Applied voltage mainly determines the interpore distance and pH defines the pore radius

3.2 MECHANISM OF PORE FORMATION IN ANODIC POROUS ALUMINA

Although many researchers in the past 35years [54-57] have studied the nucleation and growth mechanism in anodic porous alumina, even then the exact growth mechanism in the ordered porous alumina is an unanswered question. It is not clear which physical factors control the hexagonal ordering, and in particular how the surface features of the aluminum affect the regularity of pores in porous alumina. There have been several proposals to explain the mechanism of pore formation and their ordering of pores in hexagonal arrays.

Zhang et al. [58] have proposed a cellular growth mechanism in ordered porous alumina, due to oxide propagation at a curved metal-oxide interface. The regularity and

uniformity of the pores in alumina are controlled by uniformity in the arrangement of oxide cells surrounding the pores, caused by a cellular growth process. Schematic diagram of the cellular growth of porous alumina has been shown in figure 3.2

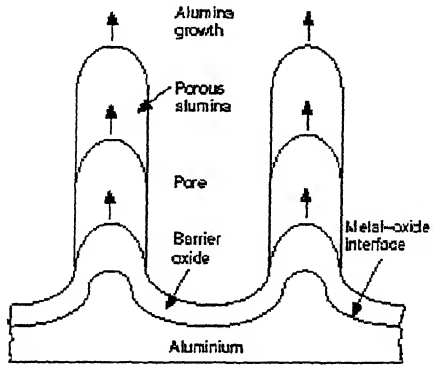

Fig. 3.2 Schematic diagram of the cellular growth of porous alumina [58]

It's clear that highly regular polycrystalline pore structures occur only for a quite small processing window, whereas an amorphous pore structure can be obtained for a very wide range of parameters without substantial change in morphology. The models based only on field distribution cannot easily explain this behavior. The self-organized arrangement of neighboring pores in hexagonal arrays can be explained by any repulsive interaction between the pores. Jessensky, Muller, and Gosele [59] have investigated the dependence of the structural properties on the anodization conditions and have given microscopic explanation of the repulsive forces operative during the anodization process. During the anodic oxidation, pores grow perpendicular to the surface with an equilibrium of field-enhanced oxide dissolution at the oxide/ electrolyte interface and oxide growth at the metal/oxide interface [60] A possible origin of forces between neighboring pores is therefore the mechanical stress which is associated with the expansion during oxide formation at the metal/oxide interface. Since the oxidation takes place at the entire pore

bottom simultaneously, the material can only expand in the vertical direction, so that the existing pore walls are pushed upwards. The aforementioned models are not able to explain the formation of pores in ordered hexagonal arrays during the anodic oxidation of Aluminum.

Thomson and Wood [45] had assumed the following mechanistic sequence :

1. Electro polishing or other pretreatment leaves a slightly scalloped surface of aluminum covered by oxide
2. A scalloped "native" barrier oxide film grew over this scalloped surface.
3. As anodization starts, pores would start at cracks and imperfections in the surface, leaving an electric field concentrated below the regions where oxide film is thinner, thus
4. Aiding the local dissolution of oxide
5. This new pore bottom deepened, and a "major" pore formed, at the expense of the former shallow pores.

At the metal/oxide interface, the average field across the barrier layer determines the barrier film growth rate, while at the oxide/electrolyte interface the local field at the pore bottom, assisted by local heating, determines the oxide dissolution rate.

The film growth rate is approximately constant and independent of pore bottom curvature. While the dissolution rate increased as the pore base radius of curvature decreased, to enlarge the pores. If the pore radius becomes too big, the dissolution slowed and the pores tended to fill. These two competing processes keep the pore radius constant. It has been suggested that, at the bottom of the pores, the p^H drops precipitously, increasing the solubility of the oxide; this is an "autocatalytic mechanism

of pit propagation". There may be pronounced temperature and concentration differential between the pore base and the bulk electrolyte. The cracks on the surface of the air-formed oxide layer can also be centers for pore nucleation, but they are unlikely to be a major factor, because of their low density.

Based on the various assumptions and proposed mechanisms in the past, the following systematic explanation is proposed;

Formation of porous anodic alumina under potentiostatic conditions starts with the creation of barrier oxide up to a thickness, determined by the applied voltage, at which the oxide becomes insulating against ionic conductions. Subsequently, pores nucleate and grow with bottoms covered by a barrier oxide layer. Finally, a regime of steady state pore growth is reached. It is characterized by balance between field enhanced oxide dissolution at the oxide/electrolyte interface at the pore bottoms and the formation of oxide at the metal/oxide interface due to migration of O^{2-}/ OH^- ions through the bottom oxide layer. The formation process is accompanied by a high starting current during formation of the initial barrier oxide. This is followed by a steep current reduction when the oxide becomes insulating against ion migration. Finally, current is increased due to the formation of the pores and ending in a constant current regime of steady pore growth.

Following are the step-by-step happenings at the molecular level during the potentiostatic anodic oxidation of aluminum;

1. Electro polishing flattens some large surface irregularities, and creates a large number of small pores. Some of these can develop into pore nuclei. Their density will decrease as pores grow, because pores merge as anodizing time increases.

2. Al^{3+} ions form at the metal/oxide interface

$Al(s) \rightarrow Al^{3+} + 3e^-$ -------(1) and migrates into the oxide layer.

3. At the oxide/electrolyte interface the water-splitting reaction occurs

$3/2\ H_2O(l) \rightarrow 3H^+(aq) + 3/2\ O^{2-}(oxide)$ --------(2)

The O^{2-} (oxide) ions migrate (due to the influence of electric field), within the oxide from the oxide/solution interface toward the metal/oxide interface, to form Al_2O_3.

4. H^+ ions generated by the water-splitting can locally dissolve oxide:

$½\ Al_2O_3(s) + 3\ H^+(aq) \rightarrow Al^{3+}(aq) + 3/2\ H_2O(l)$ ----- (3)

5. H^+ ions can also migrate toward the cathode, where they leave the electrolysis cell as H_2 gas, completing the circuit:

$3H^+(aq) + 3\ e^- \rightarrow ½\ H_2(g)$ -----(4)

By charge balance, the rates of eqs 1 and 4 must be equal.

6. Much of the oxide produced by eq 2 produces the "sidewalls" of pores. Eq 3 should be slower than eq 2

7. Eq3 occurs preferentially where the electric field is highest (at the pore bottom), i.e. at the center or close to the center of the pore bottom and keeps the barrier oxide thin.

Since, the pore walls are uniform through their length; the key growth step must be near the pore bottom, probably very close to the circle of intersection between the cylinder of the pore wall and the spherical segment of the pore bottom. At this circle of intersection water-splitting reaction (eq2) must occur. Thus the porous oxide can grow, fed by Al^{3+} ions from below and from O^{2-}(oxide) ions from "the side"

8. Pore type film starts from some Al surface that is fairly smooth (hills of at least 3nm height), but with pits formed at lattice imperfections or by electro polishing (i.e. etching or "pre- anodization"). These Al pits will be covered by an air-formed oxide, so that both the metal/oxide and the oxide/electrolyte interfaces are locally curved. The oxide thickness may be uniform or irregular: its coverage of the Al metal surface is neither perfect nor complete. This is an obvious conclusion from the observation that aluminum is macroscopically conductive despite the oxide coverage.

9. As anodization starts, the electric field at the oxide/electrolyte interface should be greater at sites where the native oxide coverage is thinner or else the metal/oxide interface flattens out initially, so that the oxide layer is thicker in some parts of the surface allowing the electric field to concentrate where the oxide is thinner.

As pore growth continues, a curved metal/oxide interface is maintained or reestablished at the pore bottom, to match the curved oxide/electrolyte interface.

Once small pores have formed, the acid and electric potential penetrate into the pore, and the growth becomes self-catalyzing.

If the pores are not ordered, then a horizontal mobility of ions in the barrier layer allows for reordering of the pore, until an equilibrium hexagonal ordering is reached. Still, a quantitative explanation for the hexagonal arrangement of pore is needed.

3.3.1 METAL IMPRIGNATION OF ALUMINA PORES

To use anodic porous alumina template for application in ultrahigh density magnetic recording and other new applications of nanostructures, the pores have to be filled with a conducting or semi conducting material, for example via electrochemical deposition. In contrast to other deposition methods like chemical vapor deposition

(CVD), during electrochemical deposition the growth of nanowires starts at the pore tips and continues in the pore direction from the pore bottom to the pore opening.

The electrochemical deposition of a metallic material on an insulating and rather thick barrier layer (1-1.2 nm per volt oxidation potential [41]) at the pore tips is not straightforward. The periodically arranged alumina structures (oxidation potential 20-195V)[48,50,51,52,59,61] exhibit a thick barrier layer. High potentials are required for the tunneling of the electrons through the barrier layer. Electrochemical by direct current (DC) is very unstable and uniform filling of the pores cannot be achieved. This is due to a cathodic side reaction, which leads to a partial removal of the barrier oxide, formation of holes in the barrier layer, and local deposition in single pores.

Until now, two different methods have been developed to obtain uniform and complete filling of pores by electro deposition. In the first method, a direct current is used for the deposition.[62] Therefore, the porous alumina needs to be detached from the aluminum substrate. Subsequently, the barrier layer is removed from the matrix structure by a chemical etching process. As a final pre-treatment step for the filling process, a metallic contact is sputtered on one side of the free-standing alumina membrane. The concept of transferring the alumina membrane is only applicable for free-standing alumina membrane that are thick (>20μm) and stable enough to be handled. For most of the nanostructure applications, a porous alumina thickness of only a few hundred nanometers is required.

The second method used for filling the alumina pores was first developed by Caboni[63-65] This method has been used for the coloration of anodic alumina in industry. Porous alumina remains on the aluminum substrate and the metal is deposited

on the barrier layer at the pore tips by an alternating deposition potential.[6,11,66,67]In this case , the production of ordered and metal-filled alumina pore structures is not limited by the thickness and size of the barrier oxide and its rectifying contact allows metal deposition by an alternating potential. Furthermore, in aqueous deposition solutions, the high cathodic potentials cause some hydrogen evolution, which may inhibit the deposition.[65,67].An alternate choice is to adopt the concept of pulsed electrodeposition(PED),[68-71] which is reliable for deposition into high aspect materials and which can compensate for the slow diffusion-driven transport in the pores.

3.3 MAGNETIC PROPERTIES OF NANOWIRES IMBEDDED IN ANODIC POROUS ALUMINA

The possible applications of magnetic nanowires imbedded in anodic porous alumina as an ultra-high density magnetic recording medium [72] has triggered several experimental studies. In the last two decades, much of the work was concerned with exploratory issues, such as establishing an easy axis for typical preparation conditions and the essential involvement of shape anisotropy, as opposed to magnetocrystalline anisotropy. More recently, attention has shifted towards the understanding of magnetization processes, which very important for the stability of recorded information.

The important length scale for such a magnetic system is the thickness of a domain wall λ_w [73,74]. Magnetic wires with diameter D_p comparable or smaller than λ_w, and a length l much larger than both can be called one-dimensional. Already in 1985, Aharoni and Shtrikman[73,74] considered theoretically the magnetization reversal processes for infinitely long cylinders and found that wires with $D_p < \sqrt{\prod} \lambda_w$ should reverse their magnetization in unison, i.e. all spins remain parallel to each other throughout the

reversal process, whereas wires wit h $D_p > \sqrt{\prod}\,\lambda_w$ should reverse via a curling mode. In both these modes all spins are reversed simultaneously, leading to a complete suppression of thermal effects for infinitely long wires. By contrast, Braun[74] showed that the formation of a spatially localized 'nucleus', that can be interpreted as a 360° - domain wall of the Neel type, leads to a finite energy barrier, even for infinitely long wires. Another possibility involving nucleation of a small volume was considered by Knowles [75], who studied the magnetization reversal of wires with a finite length. Nucleation of a single 180° - domain wall at the wire end leads to even smaller energy barriers, although this mode was predicted to occur only in wires with diameters larger than λ_w. The magnetization reversal is dominated by the nucleation process, because the domain wall(s) move very fast through the wire after their formation. Aharoni [76] showed that pinning of these domain walls can play an important role in imperfect systems. Experimental predications of these interesting theoretical predictions are not straightforward for several reasons. For Fe, Ni, and Co, λ_w is of the order of 10-50nm. In order to study one-dimensional ferromagnetic wires, the diameter of the wires should be as smaller as 10nm, preferably even smaller, and have a length in the micron range so that it can be approximated as infinite cylindrical particle. Evidently, it is not trivial to produce such wires. An often used technique is to fill a nanoporous medium with the magnetic metal by electrochemical methods. For example, Anodic porous alumina is widely used to grow arrays of high aspect metallic nanowires. There have been extensive researches in ferromagnetic nanowires in the past 5 years through out the world.

Lodder and Cheng-Zhan [77] concluded from DC-magnetization measurements in Fe-filled anodic porous alumina with D_p =60-140nm that the magnetization reversal follows

the expected curling mode. However, the direction dependence of the coercive field B_c showed a behavior different from that expected for a curling mode in individual wires. They explained the deviations as arising from dipolar interactions between the wires. To avoid these problems with interactions, Wernsdorfer et al. [78,79] applied micro-SQUID magnetometry to individual Ni nanowires with D_p = 40-140nm. They found curling behavior as well for all but their smallest wires. At $D_p \approx 40$nm, the angular dependence of the switching field indicated the development of a nucleation mode. Wang et al. [80] have investigated the dynamic properties of uniform two-dimensional arrays of nickel nanowires by inelastic light scattering.

Static and dynamic aspects of the magnetization reversal in nanowires arrays have been investigated by H. ZENG et al. [81]They have produced arrays of ferromagnetic metals(Fe, Co, and Ni) using porous anodic alumina templates ,with diameters as small as 5nm. The coercivity as a function of diameter reveals a change of the magnetization reversal mechanism from localized quasicoherent nucleation for small diameters to a localized curlinglike nucleation as the diameter exceeds a critical value determined by the exchange length.

M. ZHENG et al. [82] have studied the magnetic properties of Ni nanowires electrodeposited into self-assembled porous alumina arrays with diameter between 8 and 25nm .The coercivity measured along wire axis first increases with the wire diameter, reaches a maximum of 950Oe near a diameter of 18nm, and then decreases with further increase of wire diameter. The dependence of the magnetization of Ni nanowires is found to follow Bloch's law at low temperature but with the Bloch exponent decreasing from

the bulk value and the Bloch constant increasing from the bulk value by an order of magnitude.

In contrast to M. ZHENG et al.'s implication, K. Nielsch et al.[83] have shown that the coercivity of Ni wire having diameter of 30nm is 1200Oe along the wire axis. They have also checked the suitability of Ni nanowires arrays in Anodic Porous Alumina matrix using Magnetic Force Microscopic (MFM) analysis of magnetized and demagnetized samples. The hysteresis loops measured for the nickel nanowires array with the magnetic field applied parallel to the wire axis show a squareness of nearly 100%, which is the requirement for the media to be used for perpendicular recording. Each magnetic pillar is a single–domain magnetic particle, magnetized perpendicular to the template surface and, in principle, can store one bit of information.

CHAPTER 4

EXPERIMENTAL PROCEDURE

4.1 PREPARATION OF ANODIC POROUS ALUMINA TEMPLATES

4.1.1 Conventional method

A piece of commercial aluminum foil (90mm X 20 mm X 0.01 mm) was first degreased in acetone and rinsed in distilled water. The foil was annealed at 250°C for 2hr. The coupon of aluminum foil was mounted on a perspex sample holder (shown in figure 4.1), to avoid selective attack on the metal surface. This sample holder contains two circular holes of 15mm diameter through which aluminum is uniformly exposed to the electrolyte. Electrolyte was mechanically stirred during the anodization process to maintain the spatially homogeneous etching conditions.

During anodization, aluminum foil to be anodized was made anode while a thick stainless steel plate (8cm X 4.2cm X 0.05cm) serve as cathode. Both electrodes were placed 5cm apart in a specially designed double jacketed beaker.

Electrodes were connected to an IC Regulated DC Power supplier (Aplab7231, 0-100V, 0-1.2A). Anodization was carried out at different temperature ranging from 5°C to room temperature (25°C) at 40 V DC using 0.3M Oxalic acid as electrolyte for different lengths of time. Variation of current during the whole anodization process was measured manually.

For maintaining constant temperature of the electrolyte during the anodization process, a cold liquid (water) is being passed in the inner wall of the double jacketed

beaker using a submersible pump (Model: OASIS SX-6, VANSAL & VANSAL, KANPUR). The whole experimental setup for anodization process is shown in figure 4.2.

4.1.2 New Approach: In the present investigation, an industrially feasible and practical experimental procedure has been adopted. Flow chart of the process is shown in the figure 4.3. 200 Å thick copper was deposited on a glass substrate using vacuum deposition unit (model 12A4HD+SC) at a pressure of less than 10^{-5} torr .Over the copper film, a 500-1000 Å thick layer of Al was deposited in the same vacuum coating unit. Now, this aluminum was anodized in the same electrolytic cell as in the case of conventional method. Time of anodization is adjusted in such a way that pore bottom in alumina touches the copper layer so as to make the pore bottom electrically conducting for further metal deposition. Since, during anodization reaction at the edges is fast, lacquer was applied to protect the edges. This approach was adopted keeping in mind the process of making hard disk drive in industries.

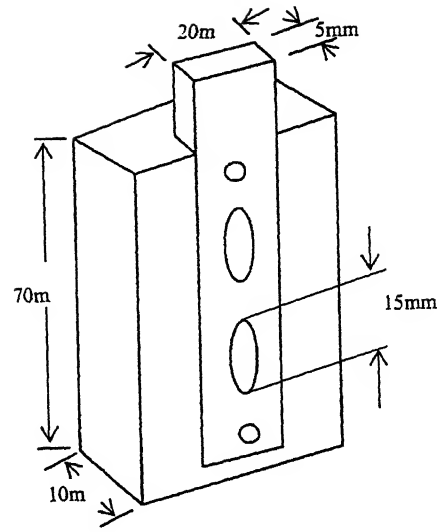

Fig 4.1 Perspex Sample Holder

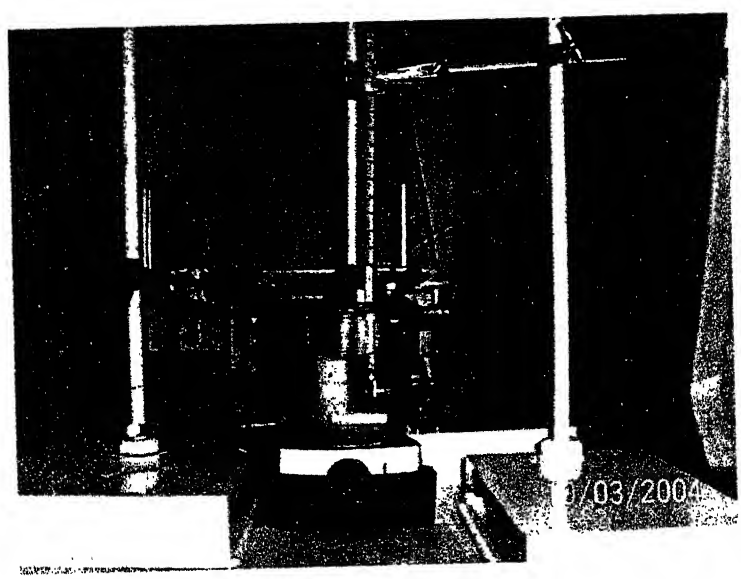

Fig. 4.2 Experimental Setup for Anodization

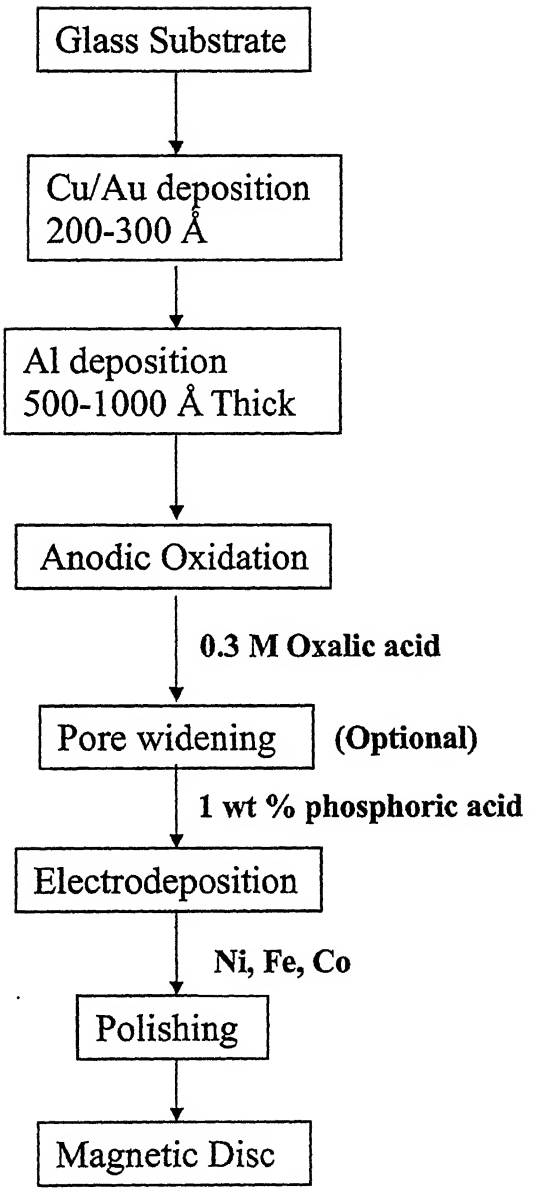

Figure 4.3: Block Diagram for the Perpendicular Media Preparation Process

4.4 ELECTRODEPOSITION OF NICKEL IN THE PORES

The pores in the as made anodic porous alumina template as well as commercially available thorough hole nanoporous alumina were filled with Nickel by pulsed electrodeposition method and AC triggered pulse at 50Hz frequency. For pulse electrodeposition method, a computer interfaced Potentiostat/Galvanostat Model263A (EG Σ G Instruments, Princeton Applied Research) was used. For supplying AC triggered pulse a SCIENTECH 1MHz function generator (ST4060) was used. Because of the low power rating of the function generator, this can't be used directly for electrodeposition process. To boost up the power rating, a power circuit was designed (shown in figure 4.4).

A circular sheet of nickel mounted on a Perspex sample holder was made as counter electrode. Nickel counter electrode was placed in vertical position so as to exactly face the targeted deposition area. It is believed that metal deposition starts at the pore bottom because of higher potential gradient prevailing at that site. The electrolyte used for the nickel deposition was so called standard Watts-bath solution [84], which is a mixture of 300g/l $NiSO_4.6H_2O$, 45 g/l $NiCl_2.6H_2O$, 45 g/l H_3BO_3, pH 4.5. During electrodeposition, the temperature of electrolyte was maintained at around 35°C.

The deposition in through hole alumina filter was done applying a modulated pulse signals in the microsecond range (Figure 4.5). On the other hand the deposition of Ni in the as made alumina template was done applying triggered AC-square wave at a frequency of 50Hz (Figure 4.6)

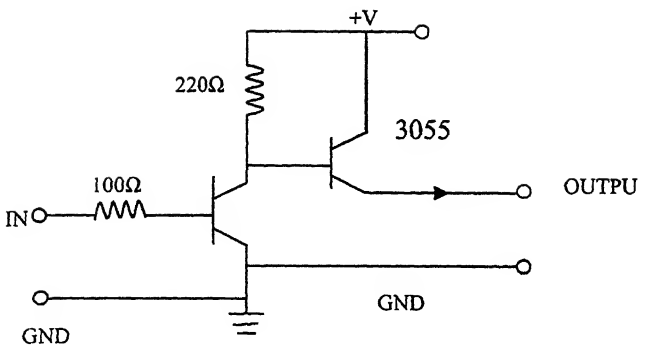

Figure 4.4: Circuit Diagram for amplification of power Rating

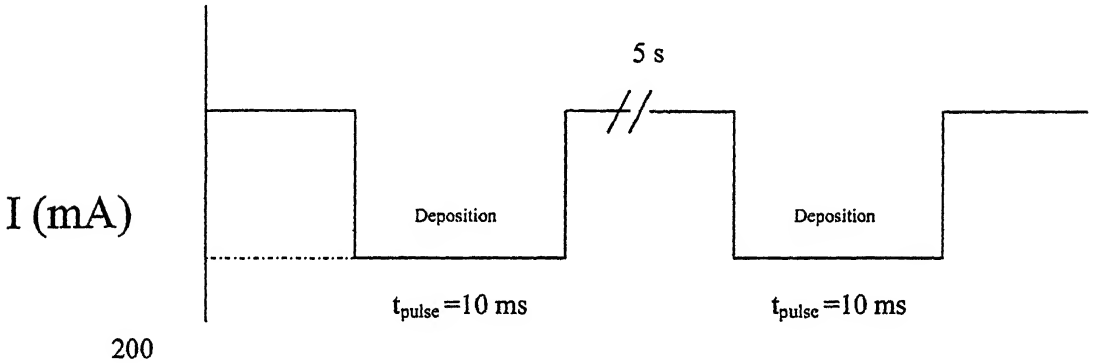

Figure 4.5: Schematic diagram of the modulated pulse signal used for filling of porous alumina template with Nickel by pulsed electrodeposition.

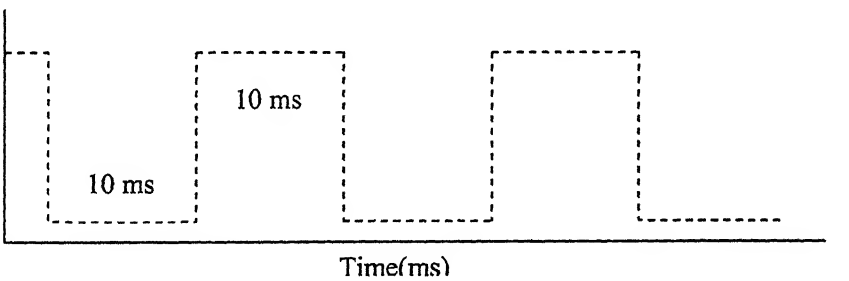

Figure 4.6: Schematic diagram of electrodeposition pulse schedule square wave at 50Hz

4.4.1. ELECTRODEPOSITION OF METAL IN THE THOROUGH HOLE ANODIC POROUS ALUMINA

As a starting material, commercially available nanoporous alumina filters were used with a thickness of 60μm. The one side of the anodic porous alumina was coated with 300 Å thick gold using vacuum coating unit at a

pressure less than 10^{-5} torr. This gold layer makes the bottom of pores electrically conducting. Before setting the sample for electrodeposition, the sample immersed in metal salt solution and was evacuated for 60minutes to remove the air bubbles inside the pore channels. This evacuation step is very important for homogeneous growth of the nanowires in the entire range of the porous alumina. If the air bubbles are trapped inside the membrane, an island of metal cluster is formed on the surface of porous alumina due to the loss of ion conduction towards the Au coated surface. The time required to completely fill up the pores with Nickel was calculated considering total integrated charge flow.

The total area exposed in the electrolyte solution during electrochemical deposition was approximately 2.27 cm^2, which can easily be enlarged to fabricate larger arrays of nanomagnets.

4.4.2 ELECTRODEPOSITION OF METAL IN THE AS MADE ANODIC POROUS ALUMINA

As made anodic porous alumina templates have thin barrier layer between bottoms of pores and remaining Al (Figure 4.8). This barrier layer blocks the dc current because of its larger resistance of 10^{10}-$10^{11}\Omega$cm.To be able to successfully fill the pores with a metal, the thickness of this barrier layer should be in between 10 and 20nm. Thus

barrier layer was thinned down by keeping the anodized sample in oxalic acid itself at around 30°C for 2hrs before electrodeposition. Alternatively, the anodized sample was dipped in 1% phosphoric acid at 40°C for different length of time to thin down the barrier layer. These processes also widen the pore diameters. It is assumed that thickness fluctuations of the barrier layer are smoothened by these treatment steps. The thinning leads to a considerable decrease in the potential barrier for the electrons to tunnel through the barrier layer, when the metal is deposited at the pore tips. Thus relatively lower voltages are required for the electrochemical filling of the pores.

To reduce the metal ions and deposit them into the pores, the alternating current is therefore imposed between the anode (alumina) and cathode. It is well known that anodic alumina conducts preferentially in only one direction i.e. in the cathode direction. Metal ions are reduced inside the pores during the cathodic half-cycles. A typical AC voltage of electro deposition of metal was 15V, at 50Hz frequency.

4.5 CHARACTERIZATION METHODS

Nanoscale materials require strict characterization of their properties for various applications. In the present investigation, Transmission Electron Microscope (TEM), Scanning Electron Microscope (SEM), X-Ray Diffraction (XRD), BET-Surface Area Measurement Technique and Vibrating Sample Magnetometer (VSM) were used for characterization of the porous alumina template and Nickel deposited porous alumina.

4.5.1 Transmission Electron Microscopy

4.5.1.1 Specimen preparation

The porous alumina pieces as such and with Nickel deposited are cut in small size of approximately 3mm X 3mm (i.e. size of TEM specimen grids) and put in the saturated solution of $HgCl_2$ for some time to dissolve the remaining aluminum at the base while leaving top alumina layer/ film intact and floating. This layer is then transferred with the help of spatula to a distilled water dish for removal of mercury molecules (if present) and if any impurity. The film is again transferred to a new dish of distilled water. This process is repeated 3-4times to yield impurity free alumina. Now, the edges of the porous alumina is protected with a lacquer and kept for drying. The protection of edges of porous alumina is necessary because the etching rate is faster at the edges than at other places. This protected porous alumina piece is transferred on 50% phosphoric acid in a dish to further thin down the specimen below 1000 Å so that electron beam can pass through. When the alumina is sufficiently thinned down, it is transferred quickly into a dish of distilled water for washing. Finally the porous alumina floating over is mounted on to the TEM specimen grid employing fine tweezers.

4.5.1.2 Specimen Observation

The alumina specimens are examined in a transmission electron microscope (Jeol JEM 2000 FX) operated at 120-160 KV. After selecting a particular area and increasing the magnification to 100KX one begins to observe the characteristic features of the sample. Firstly, the porous nature of alumina is clearly depicted in the magnified pictures. To know the insight of the pores, their size and distribution and morphology, electron micrographs are recorded at various magnifications.

Also, selected area diffraction (SAD) was taken from the region of interest to obtain crystallographic information of the film. SAD patterns contain diffused halos, indicating amorphous nature of porous alumina film.

4.5.2 Scanning Electron Microscopy

The commercial alumina filter was first characterized using JEOL JSM-840A scanning electron microscope. To examine the surface view of porous alumina small piece of filter was mounted on a conducting copper stub. For investigating cross section of the filter, filter was broken and mounted vertically in a small groove made on copper stub. Since, the porous alumina is insulating, it was coating with formless Au-Pd using sputtering technique to make the surface conducting. And the edges of the sample were applied with carbon paint so as to make electrical contact with the conducting stub.

4.5.3 BET-Surface Area Measurement

Although, the porous alumina template can be well characterized directly by electron microscopy, an indirect method is used to estimate the size distribution of pores. In this method, pore size distribution of the alumina template was determined by the conventional adsorption method.

For this analysis, more than 0.5 g of material is needed. About 25 Aluminum sheets were anodized fully so as to make them transparent. Anodized portion was collected and ground and weighed. Nitrogen isotherms were measured at the temperature of liquid nitrogen. The volume of the pores and corresponding diameter ranges were measured.

The pore size distribution is obtained by the analysis of either the adsorption or desorption isotherm. The method used is based on the BJH (Barrett, Joyner, and Halenda)

method which involves the area of the pore walls, and uses the Kelvin equation to correlate the relative pressure of nitrogen in equilibrium with the porous solid, to the size of the pores where capillary condensation takes place.

$$RT\ell n\frac{P_s}{P_o} = -2\gamma\frac{V_M}{R_K}$$

Where:

R_K= Kelvin radius

γ = adsorbate surface tension at T, in mN/m,

R= the gas constant

T=boiling point of nitrogen

V_M is the molar volume of nitrogen

Substituting for the values of the different constants and solving for R_k, one obtains:

$$R_K(nm) = 0.414\log\frac{P_s}{P_o}$$

The thickness of the nitrogen film adsorbed on the walls of the pore at a given relative pressure is calculated with the modified Halsey equation:

$$t(nm) = 0.354\times\left[\frac{5}{2.303\times\log\frac{P_o}{P_s}}\right]^{1/3}$$

The actual radius of the pore, R_P, is found by the addition of the film thickness, t to the Kelvin radius, R_k.

Mesopores within a solid adsorbent are filled progressively with adsorbate by the process of capillary condensation. Increasing numbers of molecular layers condense within increasing size of pores. When, P_s/P_o is reached near unity, all mesopores and macropores are full of liquid adsorbate.

The desorpiton isotherm is constructed by plotting the volume desorbed per gram of sample against the relative pressure, P_s/P_o .The procedure used to calculate the pore size distribution are described below.

The volume desorbed from the sample at different decreasing relative pressure values are converted to equivalent liquid volumes, because it is assumed that capillary condensation has taken place and the pores are filled with liquid rather than gas. The liquid volume is obtained by multiplying the gas volume by 0.00156(a conversion from gas at STP to liquid)

4.5.4 Vibrating Sample Magnetometry

The magnetic measurements were carried out with the help of a parallel field vibrating sample magnetometer (Princeton Applied Research Model-150A) in conjunction with a varian electromagnet model V-7200 providing a magnetic field of upto 1.1Tesla. The samples were in the form circular foil (thickness =60μm, diameter 15mm) filled with nickel metal. Around 3mm diameter disc of these foils were cut and 4-5 pieces were piled up one above another to give sufficient magnetic signal. For measurement of coercivity along the direction parallel to the plan of foil, the piled up

sample were introduced in the specimen holder horizontally with planer surface parallel to the direction of magnetic field.

For the measurement of perpendicular coercivity, first sample were kept in a cylindrical shape plastic and this was introduced vertically with planer surface perpendicular to the direction of magnetic field.

These specimens were forced to vibrate in vertical direction by a device similar to a dynamic speaker. Specimen gets magnetized by the magnetic field, which is varied in small steps. Because of the vibrations of the magnetized specimen the ac signal is induced in a pair of secondary coils placed on both sides of specimen. This signal is amplified and compared with another signal produced by a capacitor vibration exactly in the same manner. By suitable processing of the signals, an output is obtained, which is exactly proportional to the magnetic moment of the specimen. Knowing the volume or mass of the specimen, magnetization values can be obtained and net magnetization versus magnetic field cure can be plotted. A full cycle magnetization gives the hysteresis loop for which values of magnetic coercivity and net saturation magnetization were determined.

X-Ray Diffraction: The crystallinity of the nickel deposited sample and the as made alumina template was further analyzed by X-Ray diffraction (XRD).

CHAPTER 5

RESULTS AND DISCUSSION

5.1 ANODIZATION:

Anodization of aluminum foil has been carried out in acidic medium for different lengths of time at a constant voltage of 40V DC. The anodic current density was initially high (141 mA/cm^2). However, it decreased rapidly to a lowest value of $46mA/cm^2$, followed by further stabilization at a higher value of around $93mA/cm^2$. This last stable state is termed as steady-state. Initial high current is due to the metallic conducting nature of Aluminum surface. Anodization process converts the surface into a non-conducting alumina, so-called the initial barrier oxide. This caused the rapid decrease in current density. Further rise in current density results due to nucleation of pore formation. After the steady state is reached, current becomes almost constant. Measured current density vs time during anodization at room temperature (25°C) has been shown in figure 5.1. Figure 5.2 shows an alumina template/disc formed by anodization of commercial aluminum foil at 5°C in 0.3M oxalic acid electrolyte. Surrounding black region around the circular porous alumina template is the starting aluminum sheet which remained unaffected from anodic oxidation.

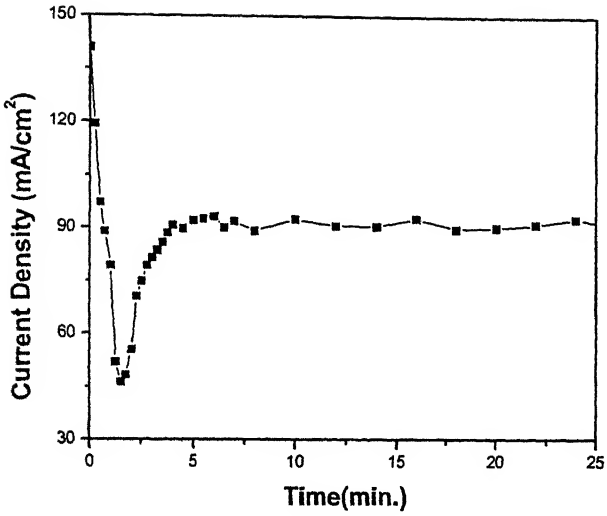

Figure 5.1. Current Density vs Time plot for anodization in 0.3M oxalic acid electrolyte at room temperature (25°C) with applied potential of 40V DC.

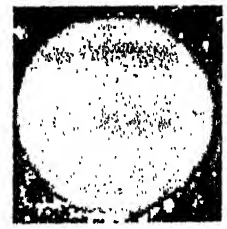

Figure 5.2. Nano porous alumina template (diameter 17mm)substrate on conducting aluminum support.

5.2 ELECTRODEPOSITION OF NICKEL IN PORES

Experimental investigations have shown that electrodeposition using direct current produces non-uniform pore-filling [67]. DC deposition requires smaller potential than for pulsed electrodeposition (PED) or AC deposition. During electrodeposition, Ni^{2+} ions move toward bottom of pores and get neutralized by electrons at alumina barrier layer (sitting on aluminum substrate) which are injected from aluminum substrate. The potential of the electrons, which drops across the barrier layer during the deposition, depends on the thickness of the barrier layer. Therefore a higher proportion of the applied deposition potential drops across the barrier layer in the case of DC deposition and thus thickness fluctuations of the barrier layer influence the deposition rate in each pore more strongly.

The formation of hydrogen can become more dominant for PED or AC deposition [67]. This effect, however, can be minimized if the deposition interfaces are being supplied sufficiently with metal ions during the course of deposition. Instead of frequently used AC deposition, the PED concept was used for the filling of porous alumina. In contrast to slow A/C volt pulses, in PED, higher current pulses can be applied. At short duration pulse, H_2 generation can be minimized. This allows better control over the deposition parameters, such as deposition rate and Ni^{2+} ion concentration at the deposition interface.

While nickel metal is deposited at the pore bottom/tip, the Ni^{2+} ions get exhausted nearby the interface of deposition site and electrolyte. Along each pore the Ni^{2+} ion concentration grows, towards electrolyte body. The metal ions, however take time to migrate from the pore opening to the pore bottom via thermal diffusion, when no

electrical stimuli is available. An attempt has been made in the investigation to estimate the ratio of the Ni^{2+} ions deposited during a single pulse and the total number of Ni^{2+} ions present in the pores (upto the length of 10μm). The following parameters were used for the calculation: concentration of metal ion c = 1.33 M, channel length h= 10μm, diameter of each pore = 40nm, pore density = 1.32 $x10^9/cm^2$, total area exposed=2.27cm^2, total current=200mA, pulse time t_{on} =10ms, and 100% current efficiency. As a result, in the area at the pore tips, 21% of all the metal ions which are present in 10μm channel, will be deposited during one pulse. Therefore, a relatively long delay time, t_{off} of 5s has been inserted between two successive deposition pulses. This t_{off} =5s was assumed to be sufficient for the concentration of metal ions at the pore tips to recover and for the deposition interfaces to be supplied with ions again, before the next deposition pulse starts. If the rate of electrodeposition is higher than that of the transport through the pores, the metal ion concentration decreases at the bottom of the pores. Consequently, hydrogen evolution becomes the dominant process, inhibiting the homogeneous deposition and decreasing the pore filling factor and the current efficiency.

5.3 TEM Studies:

5.3.1 Porous Alumina Template

The porous alumina films were observed in transmission electron microscope operating at 120KV. Figure 5.3(a-b) depict typical microstructure of porous alumina. Figure 5.3(a) show the microstructure of porous alumina obtained by anodization of Al foil (10μm thick) in 0.3M oxalic acid electrolyte at 40V. The temperature of anodization was 5°C. Clearly, the pores of quite circular shape and size are distributed all over. Pore size lies in range of 45 ±10nm with their spacing 75 ±10nm. The pore density is about

1.77×10^{11} pores/in^2. The each pore in the figure is surrounded by an average of other six nearest neighbors. At some site two pores are merged into one. This may be due to the prior mechanical stress produced due to rolling of Aluminum. Hexagonal pore arrangement in anodic alumina is formed from highly pure Aluminum foil. In the present work, purity of aluminum foil is only ~ 99.5%.

During the process of thinning down of the porous alumina film, the pore walls also dissolve and pores get widened. Thus, the pore diameter of 45nm is not the intrinsic property of porous alumina. We expect the pore diameter in the as grown porous alumina to be smaller than 40nm [46]. Pore to pore separation is the intrinsic property of the porous alumina, and remains unaltered during the thinning process.

Figure 5.3(b) shows the microstructure of porous alumina film obtained by anodizing Al thin film supported over glass slides with copper film as intermediate conducting layer. As seen, the pores in the present case are not circular. This happens due to strong surface stress arising as a result of volume change during anodic oxidation.

5.3.2 Nickel filled Porous Alumina

Attempt was made to observe tip of the nano-magnets deposited in alumina pore using gold replica method. The gold film (200Å thick), that was already deposited on one side of porous alumina template was separated by dissolving alumina matrix in HNO_3 solution. This gold replica from the nickel filled template was mounted on TEM grid. Figure 5.3(c-d) show electron micrograph of gold film supported on 200mesh grid from two different regions. The nearly circular black spots are the impression of nano magnets. Their average diameter comes to be around 25nm (averaged over 50dots).

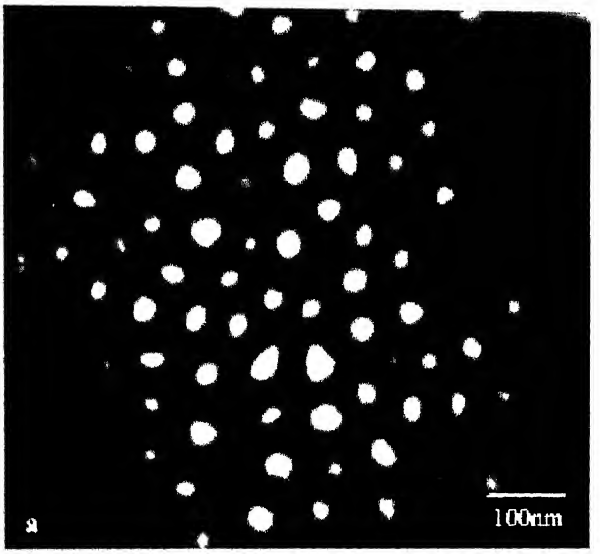

Figure 5.3(a) TEM Micrograph of porous alumina. The anodizing condition is 40V in Oxalic acid electrolyte at 5°C.

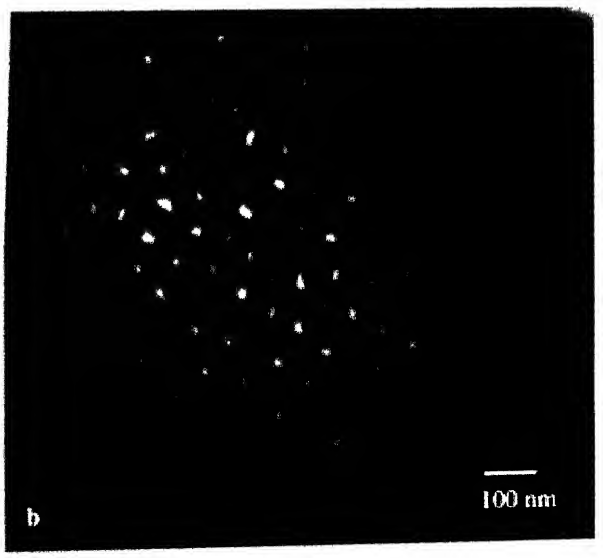

Figure 5.3(b) TEM micrograph of porous alumina. This was prepared at 40V in 0.3M oxalic acid electrolyte from thin film deposited Al on copper thin film.

5.4 SEM STUDIES:

Commercial porous alumina filter was examined by scanning electron microscopy (SEM) to determine the pore diameter, pore-to-pore separation and characteristic of pore channels. Figure 5.5 (a-b) shows the surface view of the alumina filter. Figure 5.5(a) suggests that the average diameter of the pore is 135nm (averaged over 50pores) and the average pore to pore separation is 422nm (averaged over 50 pairs of pores). The pore density is 8.5×109 /in^2. SEM images show that the array of pores is significantly away from hexagonal pattern .The porous alumina produced from indigenous aluminum show better results in terms of pore regularity than the imported porous alumna. Figure 5.5(b) shows the top view of the anodized surface at low magnification. It is evident from the figure that the pores are preferentially formed along the slip bands of rolled aluminum, indicating slip bands as the preferred sites for pore formation.

Figure 5.5(c) is an SEM images at oblique angle, at a location close to the surface showing pores opening from the top and the pore channels running from one surface to the opposite surface of alumina sheet from the side. Figure 5.5(d) shows pore-channels from the side view only. The pore channel though run together parallel to each other, they also exhibit significant bending place-to- place, indicating the presence of local stresses. It is interesting to note almost complete absence of fracture in the total course of the pore channel growth.

5.5 BET- SURFACE AREA MEASUREMENT

Figure 5.5 is a BET plot of pore volume vs pore diameter. Pore volume maxima occur at around 45nm. This result is in conformity with electron micrographic observation as shown in figure 5.3(a). Here average diameter has been found to be around 45nm. This value has however been obtained from chemically thinned alumina sheets, which is likely to cause pore widening also. There is another pore volume maximum at around 90nm. This may result, most likely, due to crushing of alumina for powdering and consequent merger of many pores together. It is needless to indicate that each maximum in pore volume is spread over almost 10nm range.

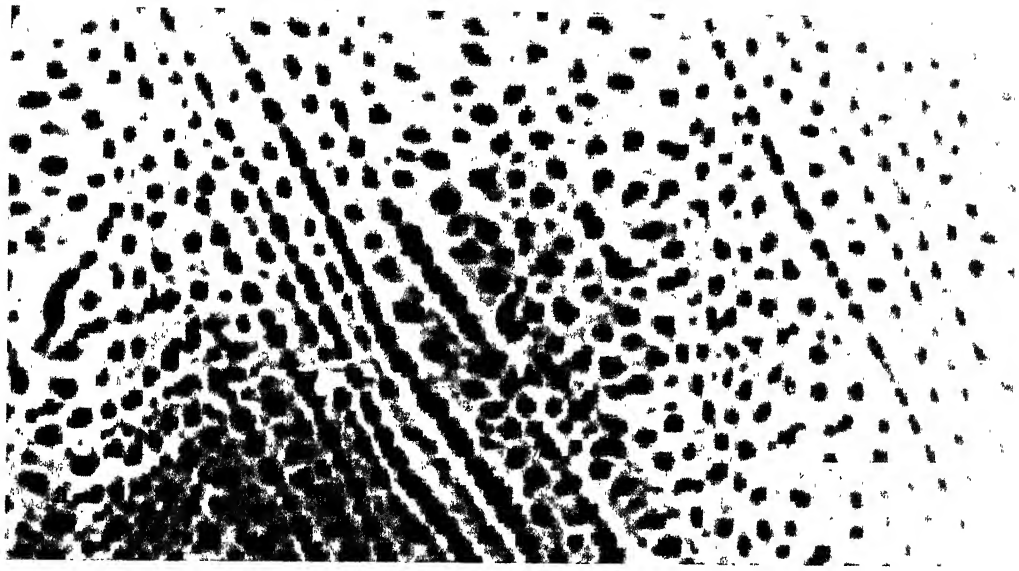

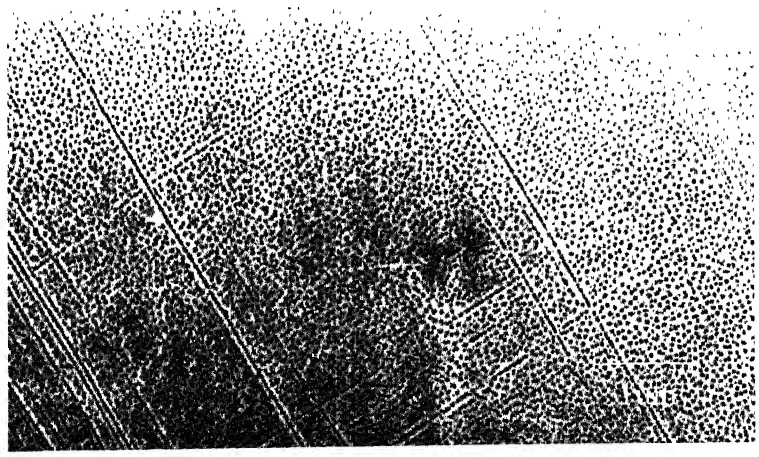

b

Figure 5.4. SEM morphologies of porous alumina filter (a) top view of the surface showing the disordered pores and (b) top view of the surface at low magnification showing that the pore are preferentially formed along the slip bands of rolled aluminum.

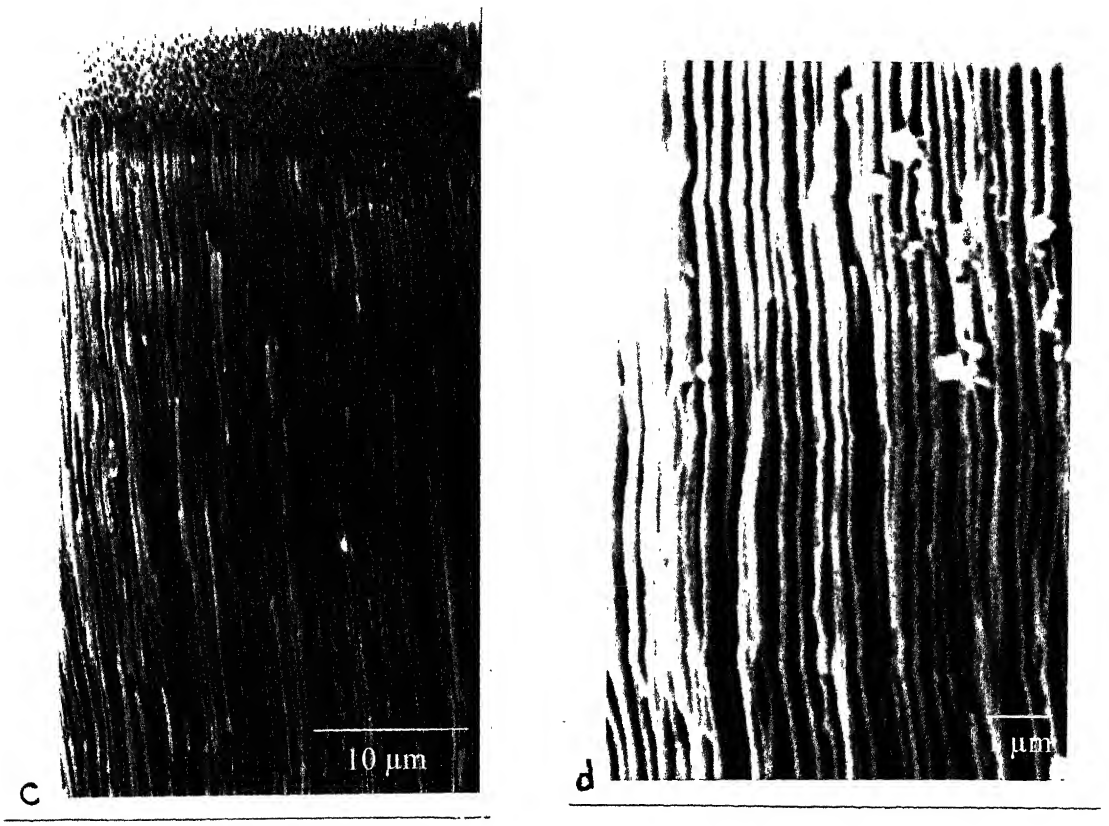

Figure 5.4. SEM morphologies of porous alumina filter(c) oblique view close to the surface and (d) cross-sectional view in the middle. The interpore distance is about 422 nm and the pore length is 60μm.

5.6 MAGNETIC MESEASUREMENTS:

Magnetic moment measurement of Nickel filled porous alumina samples was carried out with a vibrating sample magnetometer at room temperature. The objective was to investigate the coercivity of nickel nanowires perpendicular and along the plane of nickel filled alumina disc. Figure 5.1 shows a typical bulk magnetization hysteresis loop at room temperature (25°C). The external magnetic field has been applied parallel ($\|$) and perpendicular ($\perp$) to the disc plane. The imbedded nickel nanowires in the pores are nearly normal to the disc plane. The hysteresis measured with the magnetic field perpendicular to disc plane shows a high coercive field of $H_C^{\|}$ =150 Oe. The measurement with external field parallel to the disc plane shows a very low coercive field of $H_C^{\perp}$ = 25 Oe. The value of $H_c^{\|}$ (perpendicular to the disc in the present case) is at least a factor of 5-10 smaller than the values observed by other workers [32] in case of single domain nickel wires. This can be attributed to smaller aspect ratio of nickel nanowires in the present case. Also, the leftover continuous nickel film may reduce the coercive value of wires drastically. It is to be noted that the maximum H_c value (200 Oe) obtained from magnetocrystalline anisotropy is larger than the maximum value (150 Oe) obtained in the present experiment. It is therefore, possible that multidomain situation also prevails. This multidomain situation may be due the breakage of imbedded nickel nanowires into many segments. For multidomain structures, the coercive fields are determined by the pinning of domain wall type structures at grain boundaries.

The demagnetizing fields of surrounding pillars also contribute in lowering of coercive field. However, this effect is significantly reduced due to the diamagnetic nature of alumina substrate.

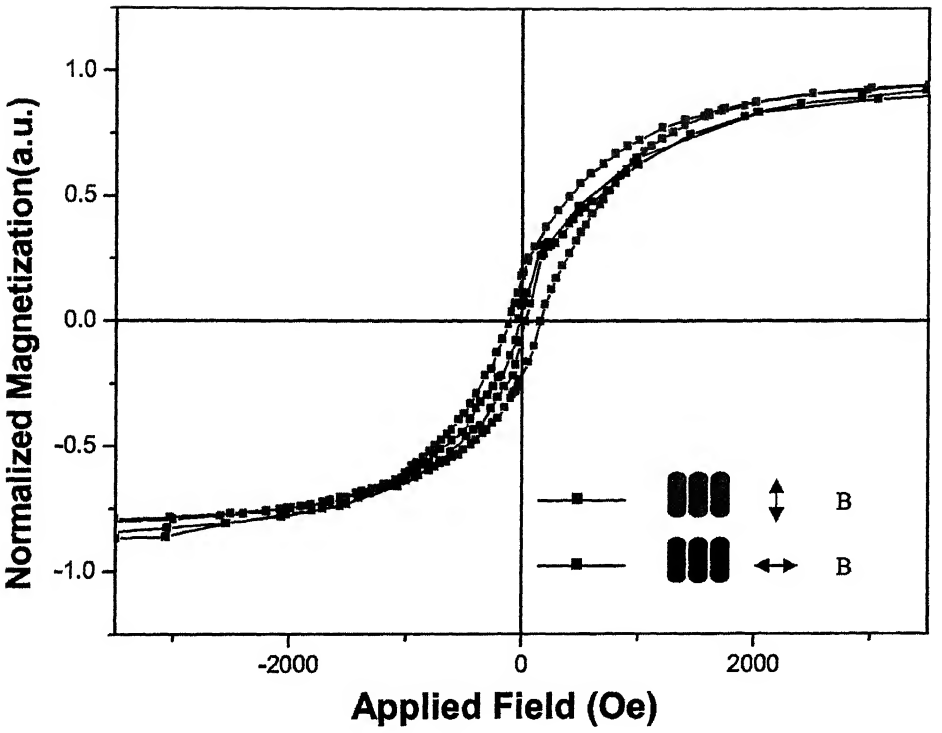

Figure 5.6: VSM hysteresis loop for self-ordered Ni nanowires array. Blue graph is for the applied magnetic field along the alumina substrate and red graph is for the applied field perpendicular to the alumina substrate.

CHAPTER6

CONCLUSIONS AND FUTURE SCOPE

6.1 CONCLUSIONS:

1. Anodic porous alumina template has been developed from indigenous aluminum by anodizing 10μm thick aluminum foil in oxalic acid electrolyte at 40V dc voltage. This porous structure consists of a pseudo hexagonally arranged cylindrical nano pores with diameter 45 ± 10nm and average period of 75 ± 10nm. This corresponds to a pore density of ~1.77 $X10^{11}$ pores/in^2.

4. Nickel can be uniformly deposited in the porous alumina template by pulsed electrochemical deposition process using standard watt type solution (300g/l $NiSO_4.6H_2O$, 45g/l $NiCl_2.6H_2O$ and 45g/l H_3BO_3) with nickel plate as a counter electrode.

5. An array of Nickel (magnetic) nanowires has been developed using nano-porous alumina template by filling the pores of the template with nickel employing pulse electrodeposition method. This array is supposed to be used for ultrahigh density (in the range of 300Gib/in^2) magnetic recording media, if the appropriate read/write head could be developed.

7. Coercivity of nickel arrays in alumina matrix shows different value along the plane of the alumina template from that perpendicular to the alumina template. Coercivity measured with the applied field perpendicular to the template is 150 Oe whereas with the

applied filed parallel to the alumina template is only 25 Oe. This can be attributed to the preferential orientation of nickel crystal in a way that <111>direction of domain is along the long axis of the nickel wires.

7. If each pore filled with magnetic particles, the media developed would correspond to an areal density of more than 177Gbit/in^2 (the current figure for magnetic hard disc areal density being 100Gbit/in^2).

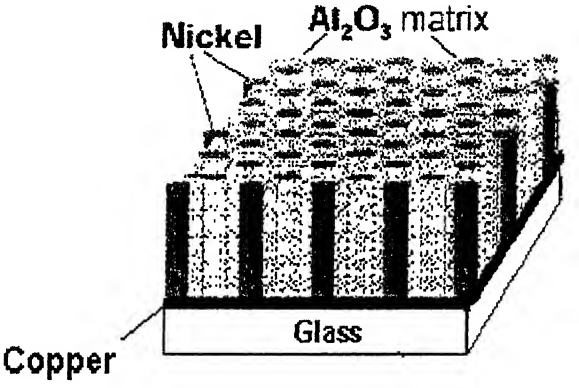

Figure 6.1 Final Product (Magnetic Disc)

6.2 OUTLOOK & FUTURE SCOPE:

Development of magnetic media based on anodic porous alumina (APA) is a new dimension. It has many advantages over thin film/particulate coated media on plane substrate. First of all, APA does not need intermediate coating as with planer substrate. The nanomagnets could be grown to almost any aspect ratio in the pores without any limitations based on achievable grain diameter 'D' to grain height 'H' ratio (D/H) as

applied filed parallel to the alumina template is only 25 Oe. This can be attributed to the preferential orientation of nickel crystal in a way that <111>direction of domain is along the long axis of the nickel wires.

7. If each pore filled with magnetic particles, the media developed would correspond to an areal density of more than 177Gbit/in^2 (the current figure for magnetic hard disc areal density being 100Gbit/in^2).

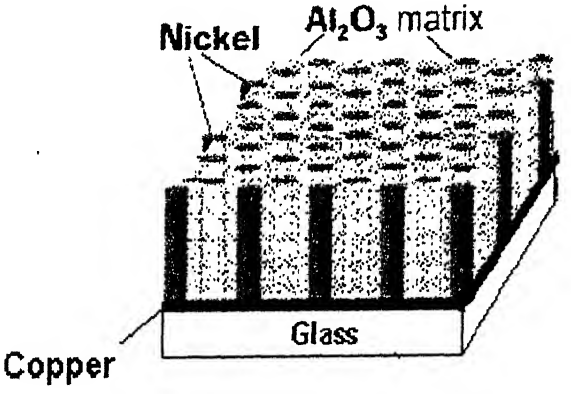

Figure 6.1 Final Product (Magnetic Disc)

6.2 OUTLOOK & FUTURE SCOPE:

Development of magnetic media based on anodic porous alumina (APA) is a new dimension. It has many advantages over thin film/particulate coated media on plane substrate. First of all, APA does not need intermediate coating as with planer substrate. The nanomagnets could be grown to almost any aspect ratio in the pores without any limitations based on achievable grain diameter 'D' to grain height 'H' ratio (D/H) as

encountered in planer media. This allows growth of very thin nanowires without compromising minimum V^* (activation volume) requirements for beyond 10years media life. The above relaxation means circumventing the thin film storage limits based on ferromagnetic to superparamagnetic transition concepts. Another important aspect is the diamagnetic effect of Al_2O_3 matrix (χ = -37 X 10^{-6} emu/gmOe) surrounding each nanomagnet. This will help in further isolation from self-demagnetization field leading to possible decrease in signal noise. In addition to all the above advantages, alumina itself is hard material just next to diamond. As a result coating process for abrasion resistance could be dispensed with and only lubrication coating will be needed. All these advantages over planer media are tempting enough to look for better ways to exploit this technique.

The battle for developing this recording media is still very grim. On one hand, it has to be adopted on glassy substrates as discs. On the other hand, it has to be deposited on polymeric tapes for relevant applications. Another important difficulty is deposition of nanomagnets in the ordered array of pores. Naturally, techniques like vacuum deposition sputtering are out of question. Electrolytic coating is the only technique suited for this work. Pure metallic nanowires of Co, Fe, and Ni can be deposited easily. However, for better stability intermetallic magnets based on CoPt, CoCrPt, CoCrPd, $CoSm_5$, $Fe_{14}Nd_2B$ having complex chemical composition are being looked for as possible candidates for storage media. Their electrodeposition will certainly raise difficulties, which have to be overcome in very near future.

REFERENCE:

1. M. P. Sharrock and L. W. Carlson, IEEE Trans. Magn., 31(1995)2871.

2. R. O'Barr, S. Y. Yamamoto, S. Schultz, W. Xu, A. Scherer, J. Appl. Phys. 81(1997)4730.

3. C. A. Ross, h. I. Smith, T. A. Savas, m. Schattenberg. M. Farhoud, M. Hwang, M. Walsh, M. C. Abraham, R. J. Ram, J. Vac. Sci. Technol. B17 (1999)3159.

4. M. Hwang, M.C. Abraham, T.A. Savas, H.I. Smith, R.J. Ram, and C.A. Ross, *J. Appl. Phys.*, **87**, 5108 (2000).

5. J. Raabe, R. Pulwey, R. Sattler, T. Schweinböck, J. Zweck, and D. Weiss, *J. Appl. Phys.*, **88**, 4437 (2000).

6. F. Li, R. M. Metzger, and W. D. Doyle, IEEE Trans. Magn. , 33, (1997)3715.

7. S. Kawai and R. Ueda, *J. Electrochem. Soc.* **122**, 32 (1975).

8. D. Al Mawlawi, N. Coombs, and M. Moskovits, *J. Appl. Phys.* **69**, 5150 (1991).

9. D.J. Sellmyer, M. Zheng, and R. Skomski, *J Phys. Condens. Mat* **13** (2001) R433.

10. K. Nielsch, R. B. Wehrspohn, J. Barthel, J. Kirschner, U. Gösele, S. F. Fischer, and H. Kronmüller, *Appl. Phys. Lett.* **79**(2001)1360.

11. D. Routkevitch, A. A. Tager , J. Haruyama, D. Almawlawi, M. Moskovits, and J. M. Xu., "Nonlithographic Nano-Wire Arrays: Fabrication, Physics, and Device Applications", IEEE Trans. Electron. Devices. 43(1996)1646.

12. W. P. Kirk and M. A. Reed, "Nanostructures and mesoscopic systems", Academic Press, New York, 1992.

13. H. Masuda and M. Satoh, "Fabrication of Gold Nanodot Array Using Anodic Porous Alumina as an Evaporation Mask" Jpn. J. Appl. Phys., 35(1996) L126.

14. M. Saito, M. Kirihara, T. Taniguchi, and M. Miyagi, Appl. Phys. Lett. 55 (1994) 607.

15. D Routkevitch, T. Bigioni, M. Moiskovits, and J. M. Xu, J. Phys. Chem., 100 (1996) 14037.

16. C. J. Miller and M. Majda, J. Am. Chem. Soc. 107 (1985) 3118.

17. S. Iwasaki, IEEE Trans. Magn. , Vol. MAG-16 (1980) 71.

18. H. N. Bertram and M. Williams, IEEE Trans. Magn. 36(2000)1.

19. D. Weller and A moser, IEEE Trans. Magn., 35(1999) 4423.

20. R. M. White, "Introduction to Magnetic Recording" IEEE Press, New York (1984)

21. E. Grochowski and D. A. Thomson, IEEE Trans. Magn. 30(1994) 3797.

22. E. Growchowski and R. Hoyt, IEEE Trans. Magn. 32(1996)1850.

23. L. Neel "Theorie do trainage magnetique" Ann Goephy 5 (1949)99.

24. H. Zeng, R. Skomski and L. Menon, Y. Liu, S. Bandyopadhyay, and D. J. Sellmyer, Phys. Rev. B 65 (2002)134426.

25. H. N. Bertram, M. K. Stafford and D. R. Mills, J. Audio Eng. Soc. 28 (1980)690.

26. K. B. Kloassen, R. G. Hirko and J.T. Contreras, IEEE Trans. Magn. 34 (1998) 1822.

27. C. H. Back, D.Weller, J. Heidmann, D.Mauri, D. Guarisco.E.L.Garwin and H.C. Siegmann "Magnetization Reversal in Ultrashort Magnetic Field Pulses" Phys. Rev. Lett. 81(1998)3251.

28. H. C. Siegmann, E. L. Garwin, C. Y. Prescott, J. Heidmann, D. Mauri, D. Weller, R. Allenspach, and W. Weber, "Magnetism with picosecond field pulses," J. Magnetism Magn. Mater. 151(1995) L8.

29. C. H. Back, R. Allenspach, W. Weber, S. S. P. Parkin, D. Weller, E. L. Garwin, and H. C. Siegmann, "Minimum field strength in ultrafast magnetization reversal," *Science*, Aug. 5(1999).

30. G. Ju, A. V. Nurmikko, R. F. C. Farrow, R. F. Marks, M. J. Carey and B. A. Gurney "Ultrafast Time Resolvedphotoinduced magnetization rotation in a ferromagnetic/antiferromagnetic exchange coupled system." Phys. Rev. Lett., 82(1999)3705.

31. B. Slutsky and H. N. Bertram, IEEE Trans. Magn. 30 (1994)2808.

32. K. Nielsch, R. B. Wehrspohn, S. F. Fischer, H. Kronmuller, J. Barthel, J. Kirschner, T. Schweinbock, D. Weiss, and U. Gosele, Mat. Res. Soc. Symp. Proc. 705 (2002)Y9.3.1

33. R. M. Metzger, Valery V. Konovalov, M. Sun, T. Xu, G. Zangari , B. Xu, M. Benakli, and W. D. Doyle, IEEE Trans. Magn. 36 (2000) 30.

34. Xiaohua, Feiyhe Li and Robert M. Metzger, "Synthesis and magnetic properties of Electrodeposted Metal Particles on Anodic Alumina" J. Appl. Phys. 79(1996)4866.

35. M. Shiraki, Y. Wakui, T. Tokushima and N. Tsuya, IEEE Trans. Magn. MAG 21 (1985)1465.

36. K. N. Nielsch, R. B. Wehrspohn, J. Barthel, J. Kirschner, S. F. Fischer, h. Kronmuller, T. Schweinbock, D. Weiss, U. Gosele, J. Magn. Magn. Mat. 249 (2002) 234.

37.

38. K. Douglas, G. Devausd and N. Clark, Science 257(1992)642.

39. M. Park, C. Harrison, P.M. Chaikin, R. A. Register and D. H. Adamson, Science 276 (1997)1401

40. M. Green, M. G-Parajo, F. Khaleque and R. Murray, Appl. Phys. Lett. 62 (1993) 264.

41. F. Keller, M. S Hunter, and D. L. Robinson, J. Electrochem. Soc. 100(1953)411.

42. J. P. O'Sullivan and G. C. Wood, Proc. Roy. Soc. Lond A 317(1970)511.

43. J. W. Diggle, T. C. Downie, and c. w. Goulding, Chem. Rev. 69 (1969) 365.

44. K. N. Rai and E. Ruckenstein, J. Catal. 40 (1975)117.

45. G. E. Thompson, G. C. Wood, Nature 290(1981)230.

46. H. Hasuda and K.Fukuda, Science 268(1995) 1466.

47. H. Masuda and M. Satoh, Jpn. J. Appl. Phys. 35 (1996) L126.

48. H. Masuda, F. Hasegwa and S. Ono, J. Electrochem. Soc. 144 (1997) L127.

49. H. Masuda, H. Yamada, M. Satoh, H. Asoh, M. Nokao, and T. Tamamura, Appl. Phys. Lett. 71(1997)2770.

50. O. Jessensky, F. Muller, and U. Gosele, J. Electrochem. Soc. 145 (1998)3735.

51. A. P. Li, F. Muler, A. Birner, K. Nielsch, and U. Gosele, J. Appl. Phys. 84 (1998)6023.

52. H. Masuda, K. Yada and A. Osaka, 37(1998) L1340.

53. K. Nielsch, J. Choi, K. Schwirn, R. B.Wehrspohn, and U. Gosele, Nano Lett., Vol. 0, No. 0 (2002)A-D.

54. J. W. Diggle, in "Oxides and oxide films", Vol. 2(ed.) (Dekker, New York, 1973) pp. 281.

55. G. E. Thompson, R. C. Furneaux, G. C .Wood, J. A. Richardson, and J. S. Goode, Nature 272(1978)433.

56. K. Shimizu, K. Kobayashi, G. E. Thompson and G. C. Wood, Phil. Mag. A 66 (1992) 643.

57. V. V. Yuzhakov, H. C. Chang, A. E. Miller, Phys. Rev. B56(1997)12608.

58. L .Zhang, H. S. Cho, F. Li, R. M. Metzger, W. D. Doyle, J. Mat. Sc. Lett. 17 (1998) 291.

59. O. Jessensky, F. Muller, and U. Gosele, Appl. Phys. Lett. 72(1998)1173.

60. V. P. Parkhutik and V. I . Shershulsky, J. Phys. D: Appl. Phys. 25 (1992) 1258.

61. A. P. Li, F. Müller, A. Birner, K. Nielsch, U. Gösele, Adv. Mater. 11(1999) 483.

62. H. Masuda, M. Yotsuya, M. Ishida, Jpn. J. Appl. Phys. 37(1998) L1090.

63. V. Caboni, Italian Patent 339 232, 1936.

64. Langbein-Pfandhauser GmbH, German Patent 741 753, 1940.

65. W. Sautter, G. Ibe, J. Meier, Aluminium 50(1974) 143.

66. D. Al Mawlawi, N. Coombs, M. Moskovits, J. Appl. Phys. 70(1991)4421.

67. D. Routkevitch, J. Chan, J. M. Xu, M. Moskovits, Electrochem. Soc. Proc. Ser. 1997, PV 97-7, 350.

68. J. C. Puippe, F. Leaman, Theory and Practice of Pulse Plating, AESF, Orlando 1986.

69. G. McMahon, U. Erb, Microstruct. Sci. 17(1989), 447.

70. H. Natter, M. Schmelzer, R. Hempelmann, J. Mater. Res. 13(1998)1186.

71. P. T. Tang, T. Watanabe, J. E. T. Andersen, G. Bech-Nielsen, J. Appl. Electrochem. 25(1995) 347.

72. N. Tsuya, Y. Saito, H. Nakamura, S. Hayano, A. Furugohri, K. Ohta, Y. Wakui, T. Tokushima, J. Magn. Magn. Mater. 54-57 (1986) 1681.

73. E.H. Frei, S. Shtrikman, D. Treves, Phys. Rev. 106 (446)1957.

74. A. Aharoni, S. Shtrikman, Phys. Rev. 109 (1958) 1522.

75. H.-B. Braun, Phys. Rev. Lett. 71(1993) 3557.

76. J.E. Knowles, J. Magn. Magn. Mater. 61 (1986) 121.

77. G.T.A. Huysmans, J.C. Lodder, J. Wakui, J. Appl. Phys. 64 (1988) 2016.

78. M. E. Schabes, J. Magn. Magn. Mater. 95 (1991) 249. ... Lett. 77 (1996) 1873.

79. J.C. Lodder, L. Cheng-Zhang, IEEE Trans. Magn. 25(1989) 4171.

80. W. Wernsdorfer, K. Hasselbach, A. Benoit, B. Barbara, B. Doudin, J. Meier, J.Ph. Ansermet, D. Mailly, Phys. Rev.B 55(1997)11552.

81. H . Zeng, R. Skomski, L. Menon, Y. Liu, S. Bandyopadhyay, and D. J. Sellmyer, Phys. Rev. B 65,(2002)134426.

82. M. Zheng, L. Menon,H. Zheng, Y. Liu, S. Bandyopadhyay, R. D. Kirby, and D. J. Sellmyer, Phys. Rev. B 62,(2000)12282.

83. K. Nielsch, R. B. Wehrspohn, J. Barthel, J. Kirschner, S. F. Fischer, H. Kronmuller, T. Schweinbock, D. Weiss, U. Gosele, J. Magn. Magn. Mater. 249(2002)234.

84. O. P. Watts, Trans. Am. Electrochem. Soc. 29(1916)395.

A 148439

Date Slip

This book is to be returned on the date last stamped.

.....	.....
.....	.....
.....	.....
.....	.....
.....	.....
.....	.....
.....	.....
.....	.....
.....	.....
.....	.....
.....	.....